KNS4/UPEX1: A Type II Arabinogalactan β-(1,3)-Galactosyltransferase Required for Pollen Exine Development[1][OPEN]

Toshiya Suzuki[2], Joan Oñate Narciso[2,3], Wei Zeng, Allison van de Meene, Masayuki Yasutomi, Shunsuke Takemura, Edwin R. Lampugnani, Monika S. Doblin[4], Antony Bacic[4], and Sumie Ishiguro[4]*

Graduate School of Bioagricultural Sciences, Nagoya University, Nagoya 464-8601, Japan (T.S., M.Y., S.T., S.I.); and ARC Centre of Excellence in Plant Cell Walls, School of BioSciences, University of Melbourne, Victoria 3010, Australia (J.O.N., W.Z., A.v.d.M., E.R.L., M.S.D., A.B.)

ORCID IDs: 0000-0002-3666-7240 (E.R.L.); 0000-0002-8921-2725 (M.S.D.); 0000-0001-7483-8605 (A.B.); 0000-0002-6160-7434 (S.I.).

Pollen exine is essential for protection from the environment of the male gametes of seed-producing plants, but its assembly and composition remain poorly understood. We previously characterized Arabidopsis (*Arabidopsis thaliana*) mutants with abnormal pollen exine structure and morphology that we named *kaonashi* (*kns*). Here we describe the identification of the causal gene of *kns4* that was found to be a member of the CAZy glycosyltransferase 31 gene family, identical to *UNEVEN PATTERN OF EXINE1*, and the biochemical characterization of the encoded protein. The characteristic exine phenotype in the *kns4* mutant is related to an abnormality of the primexine matrix laid on the surface of developing microspores. Using light microscopy with a combination of type II arabinogalactan (AG) antibodies and staining with the arabinogalactan-protein (AGP)-specific β-Glc Yariv reagent, we show that the levels of AGPs in the *kns4* microspore primexine are considerably diminished, and their location differs from that of wild type, as does the distribution of pectin labeling. Furthermore, *kns4* mutants exhibit reduced fertility as indicated by shorter fruit lengths and lower seed set compared to the wild type, confirming that KNS4 is critical for pollen viability and development. KNS4 was heterologously expressed in *Nicotiana benthamiana*, and was shown to possess β-(1,3)-galactosyltransferase activity responsible for the synthesis of AG glycans that are present on both AGPs and/or the pectic polysaccharide rhamnogalacturonan I. These data demonstrate that defects in AGP/pectic glycans, caused by disruption of *KNS4* function, impact pollen development and viability in Arabidopsis.

Pollen, the male gametophyte of all seed plants, is crucial for reproductive success. Due to the harsh environmental conditions that pollen must survive in, it has developed an elaborate and specialized cell wall. However, despite its importance our knowledge of the fine structure and assembly of the pollen grain wall is poorly understood (Newbigin et al., 2009; Ariizumi and Toriyama, 2011; Quilichini et al., 2015; Shi et al., 2015). Arabidopsis (*Arabidopsis thaliana*) provides an ideal genetic and cell biological model to dissect the assembly of the components of the pollen grain wall. Arabidopsis pollen grains have a typical surface structure that consists of an inner intine layer, which is usually made up of cellulose and pectin, and the outer exine, which is largely composed of sporopollenin (Li et al., 1995). The exine is further subdivided into inner nexine and outer sexine. The sexine has a three-dimensional (3D) structure composed of many columns called baculae and a roof called tectum. These two structures give the Arabidopsis pollen surface a reticulate appearance with a uniform mesh size. The nexine is composed of outer nexine I (foot layer), which contains sporopollenin, and inner nexine II (endexine; Ariizumi and Toriyama, 2011; Jiang et al., 2013). A recent study suggests that arabinogalactan proteins (AGPs) are key constituents of nexine with expression of *AtAGP6* in the nexine-deficient mutant *transposable element silencing via at-hook* (*tek*) partially restoring nexine formation (Jia et al., 2015). The materials comprising the exine are derived

[1] This work was supported by KAKENHI grant no. 20000304 (to T.S.); grants no. 21024004, 23370018, and 15H01229 (to S.I.) from the Ministry of Education, Culture, Sports, Science and Technology/Japan Society for the Promotion of Science (MEXT/JSPS), Japan; grant no. CE1101007 (to W.Z., E.R.L., A.v.d.M., M.S.D., and A.B.) from the Australia Research Council (ARC) to the ARC Centre of Excellence in Plant Cell Walls; and the University of Melbourne under the Melbourne International Research Scholarship (MRS) and Melbourne International Fee Remission Scholarship (MIFRS) (to J.O.N.).

[2] These authors contributed equally to the article.

[3] Present address: Faculty of Agriculture and Life Sciences, Lincoln University, Lincoln 7647, New Zealand.

[4] These senior authors contributed equally to the article.

* Address correspondence to guronyan@agr.nagoya-u.ac.jp.

The author responsible for distribution of materials integral to the finding presented in this article in accordance with the policy described in the Instructions for Authors (www.plantphysiol.org) is: Sumie Ishiguro (guronyan@agr.nagoya-u.ac.jp).

T.S., J.O.N., S.I., M.S.D., and A.B designed the research; T.S., J.O.N., W.Z., A.v.d.M, M.Y., S.T., E.R.L., and S.I. performed the research; all authors contributed to the analysis of the data and the writing of the article.

[OPEN] Articles can be viewed without a subscription.

www.plantphysiol.org/cgi/doi/10.1104/pp.16.01385

from the cells of the tapetum and the deposition pattern of the exine is determined during the tetrad stage (Zhou et al., 2015). Surrounding the outer exine layer is the pollen coat, containing proteins and lipids that accumulate in the exine cavities (Quilichini et al., 2015).

Exine is composed of sporopollenin, a structurally robust biopolymer made from aliphatic and aromatic precursors (Ariizumi and Toriyama, 2011; Quilichini et al., 2015). Sporopollenin precursors are synthesized mainly in tapetal cells and transported to the microspore surface by the involvement of many genes in which mutations often cause strong defects in exine development. These genes include: *MALE STERILITY2* (*MS2*) (Aarts et al., 1997), *FACELESS POLLEN1* (*FLP1*) (Ariizumi et al., 2003), *NO EXINE FORMATION1* (*NEF1*) (Ariizumi et al., 2004), *CYP703A2* (Morant et al., 2007), *ACYL-CoA SYNTHETASE5* (*ACOS5*) (de Azevedo Souza et al., 2009), *LESS ADHERENT POLLEN3* (*LAP3*), *LAP5/POLYKETIDE SYNTHASE B* (*PKSB*), *LAP6/POLYKETIDE SYNTHASE A* (*PKSA*) (Dobritsa et al., 2009a; Dobritsa et al., 2010; Kim et al., 2010), *CYP704B1* (Dobritsa et al., 2009b), *DIHYDROFLAVONOL 4-REDUCTASE-LIKE1* (*DRL1*)/*TETRAKETIDEα-PYRONE REDUCTASE2* (*TKPR2*) (Tang et al., 2009; Grienenberger et al., 2010), *TKPR1* (Grienenberger et al., 2010), and a member of ATP-binding cassette transporter gene *ABCG26* (Quilichini et al., 2010; Choi et al., 2011; Dou et al., 2011; Kuromori et al., 2011). Although many of these genes are specifically expressed in tapetal cells, it has been proposed that microspores also synthesize and secrete sporopollenin at the initial stage of exine development in tetrads (Wallace et al., 2011).

Exine development is initiated with the formation of primexine, a layer of matrix between the microspore plasma membrane and callosic wall that temporarily separates the microspores in the pollen tetrad (Heslop-Harrison, 1968; Owen and Makaroff, 1995; Paxson-Sowders et al., 1997). Primexine is believed to act as a scaffold for the attachment of sporopollenin monomers (Ariizumi and Toriyama, 2011). After primexine formation, undulation of the microspore plasma membrane occurs, which contributes to determining the position of bacula formation (Paxson-Sowders et al., 1997; Zhou et al. 2015). An Arabidopsis gene, *DEFECTIVE IN EXINE FORMATION1* (*DEX1*), encodes a membrane-associated protein required for primexine development and plasma membrane undulation, and a mutation of the gene results in random deposition of sporopollenin at the plasma membrane surface (Paxson-Sowders et al., 1997; Paxson-Sowders et al., 2001). Mutants of *TRANSIENT DEFECTIVE EXINE1* (*TDE1*)/*DE-ETIOLATED2* (*DET2*) revealed the involvement of brassinosteroids in primexine formation (Ariizumi et al., 2008). The callosic wall in tetrads also plays a crucial role in exine development. Mutations in *CALLOSE SYNTHASE5* (*CALS5*)/*GLUCAN SYNTHASE LIKE2* (*GSL2*) cause a severe defect in exine development despite normal deposition of primexine (Dong et al., 2005; Nishikawa et al., 2005). Furthermore, *RUPTURED POLLEN GRAIN1* (*RPG1*), *NO PRIMEXINE AND PLASMA MEMBRANE UNDULATION* (*NPU*), and *EXINE FORMATION DEFECT* (*EFD*) are required for *CALS5/GSL2* expression, primexine deposition, and plasma membrane undulation (Guan et al., 2008; Chang et al., 2012; Sun et al., 2013; Hu et al., 2014). Mutations in these genes almost completely abolish the structure of exine and often affect the viability of pollen grains.

Despite the accumulating knowledge about sporopollenin synthesis, little is known about how the 3D structure/organization of exine is formed (Quilichini et al., 2015; Shi et al., 2015). To identify the genes determining exine structure, we previously screened an EMS-mutagenized population of Arabidopsis by scanning electron microscopy (SEM) and identified 12 mutants, named *kaonashi* (*kns1* to *kns12*), showing abnormal exine morphology and classified them into four types (Suzuki et al., 2008). Type-1 mutants showed collapsed exine structures whereas type-2 mutants make a remarkably thin exine. The type-3 mutants showed defective tectum formation and the type 4 mutants showed densely distributed baculae. All identified *kns* mutants are recessive, suggesting that these *KNS* genes are expressed in diploid cells (Suzuki et al., 2008). In this article, we focus on a unique type-2 mutant, *kns4*, in which the exine is less than half the thickness of wild type but still has a reticulate structure. Another characteristic of *kns4* is that mature pollen grains of the mutant often aggregate (Suzuki et al., 2008).

A similar genetic screen was carried out by Dobritsa et al., (2011) with an Arabidopsis T-DNA insertion population and many mutants with a variety of defects in exine structure were found. For example, the exine of *spongy2* (*spg2*) has irregularly distributed and elongated tectum elements and lacunae (holes within the tectum) of variable size and shape. Another mutant, *uneven pattern of exine1* (*upex1*), shows a grossly disorganized exine (Dobritsa et al., 2011). Only part of the *upex1* pollen surface maintains a reticulate structure; other areas either lack exine or have essentially smooth exine with small lacunae (Dobritsa et al., 2011). Observations at high magnification revealed that the *upex1* exine consisted of very short baculae and an overdeveloped tectum that had fewer and smaller lacunae than in the wild type (Dobritsa et al., 2011). The gene underlying the *upex1* mutation was identified as *At1g33430*, a gene that is expressed specifically in anthers at bud stages **9** to **10** when exine development occurs in microspores (Dobritsa et al., 2011).

During microspore development, many kinds of cell walls are successively synthesized and degraded in the following sequence. In Arabidopsis, the primary cell wall of the pollen mother cell (PMC) characteristically contains methylesterified pectin (homogalacturonan, HG) and AGPs (Rhee and Somerville, 1998; Coimbra et al., 2007). Beneath the PMC primary wall, a callosic wall forms that becomes thicker in tetrads and separates the microspores generated by meiosis. In the

tetrad, microspores form a layer of primexine matrix consisting of at least methylesterified HG and rhamnogalacturonan II (RG-II; Rhee and Somerville, 1998), and exine construction is initiated in the primexine. Enzymatic degradation of the PMC primary cell wall and callosic wall occurs and the microspores are released into the locular space. Free microspores are still coated with a layer of pectic polysaccharides (also referred to as "primexine" in the literature), although the pectin undergoes demethylesterification (Rhee and Somerville, 1998). Intine forms beneath the exine, and two rounds of mitotic cell division produce two sperm cells surrounded by an AGP-containing wall (Coimbra et al., 2007). The intine in mature pollen grains consists mainly of cellulose, noncellulosic polysaccharides, and pectin (van Aelst and van Went, 1992; Ariizumi and Toriyama, 2011), whereas an intine-like structure ("germination plaque") produced upon pollen germination consists of cellulose, callose, and partly demethylesterified pectin (Hoedemaekers et al., 2015), with the pollen tube wall also including AGPs (Nguema-Ona et al., 2012).

AGPs are a class of Hyp-rich glycoproteins found ubiquitously in plant cell walls, secretions, and at the plasma membrane (Nguema-Ona et al., 2012). Most members of this family of proteins are defined by a Hyp-rich protein backbone decorated by type II AGs, that is, a galactan backbone of β-(1,3)-linked-D-galactopyranose residues, with branches (between one and three residues long) of β-(1,6)-linked-D-galactopyranose, as well as other terminal monosaccharides such as Fuc, GlcA, and rhamnose, among others (Ellis et al., 2010). AGPs (mostly through their β-(1,3)-galactan backbone) have the ability to bind selectively to and be precipitated by $(\beta\text{-D-glucosyl})_3$ and $(\beta\text{-D-galactosyl})_3$ Yariv reagents (Fincher et al., 1983). These reagents are widely used to perturb the molecular functions of AGPs as well as for their detection, quantification, purification, and staining (Fincher et al., 1983).

AGPs are proposed to have a wide variety of functions and play a pivotal role in plant growth and development, particularly in sexual reproduction (for review, see Ellis et al., 2010; Tan et al., 2012). In light of the observation that AGP epitope-directed antibodies show a differential spatio-temporal distribution pattern during both anther and ovule development, it has been suggested that AGPs could be used as gametophytic cell differentiation markers (Coimbra et al., 2007). A few AGPs, for example, *AtAGP6* and *AtAGP11*, have been implicated in pollen development (Coimbra et al., 2009). A double null *agp6 agp11* mutant has collapsed pollen grains, reduced (and precocious) pollen grain germination and tube elongation, and displays shorter fruits with less seeds; these phenotypes are due to pollen abortion (Coimbra et al., 2009, 2010).

BLAST searches of the Arabidopsis genome using mammalian β-(1,3)-GalT sequences as queries identified 20 genes of the CAZy Glycosyltransferase (GT) 31 family (www.cazy.org/) as potentially being involved in the synthesis of the type II AG backbone of AGPs (Qu et al., 2008). Based on phylogenetic analysis, the Arabidopsis GT31 family GalTs were grouped into four clades [clades 1 (VIII and IX), 7 (V and VI), 10 (I to IV), and 11 (VII); Qu et al., 2008; Egelund et al., 2011]. Subsequently, several Arabidopsis GT31 clades 7 and 10 members have been shown to have AGP-glycan synthase activity: *AtGALT2*, *3*, *4*, *5*, and *6* (clade 7; Basu et al., 2013; Basu et al., 2015), *AtGALT31A* (Geshi et al., 2013), as well as three Hyp O-*GALT*s, *HPGT1*, *2*, and *3* (clade 10; Ogawa-Ohnishi and Matsubayashi, 2015). In addition to biochemical activity assay data, aberrant growth phenotypes, in varying degrees of severity, have been observed in the aforementioned loss-of-function *galt* mutants. Hence, both biochemical and genetic evidence exists supporting the view that the AG glycan moieties of AGPs are critical for their biological functions.

In this study, we used genetic and cell biology approaches to identify and characterize *KNS4*. The gene was found to be *At1g33430*, a clade 10 member of the GT31 family (Egelund et al., 2011), and identical to *UPEX1* (Dobritsa et al., 2011). Heterologous expression and in vitro enzymatic activity assays provided biochemical evidence that KNS4 is a β-(1,3)-GalT likely synthesizing the β-(1,3)-galactan backbone of AGPs and/or the side-chains of RG-I. Immunolabeling and β-Glc Yariv staining show that *kns4* mutants have reduced AGP content in the primexine of developing microspores, suggesting AGPs play an important role in this structure. Furthermore, *kns4* mutants exhibit pollen aggregation and reduced fertility, as indicated by shorter fruit lengths and lower seed set compared to the wild type, confirming that KNS4 is critical for pollen development.

In the accompanying article by Li et al. (2017), the characterization of two exine mutants, *upex1* and *spg2*, is reported. They showed that *SPG2* (*At1g27600*) encodes the previously characterized IRREGULAR XYLEM9-LIKE (*IRX9L*) GT 43 protein involved in xylan backbone synthesis and that xylan, as well as AGP, is a component of the primexine wall (Li et al., 2017). Thus, our complementary articles provide evidence that AGPs, pectins, and xylans in primexine contribute to the deposition of sporopollenin onto the microspore surface, and to the construction of a regular reticulate exine pattern.

RESULTS

Identification of the *KNS4* Gene

The causative mutation of the EMS-induced *kns4* mutant (hereafter *kns4-1*) was previously reported to be mapped to chromosome 1 (Suzuki et al., 2008). Using a PCR marker approach, the *kns4-1* mutation was mapped further to a 300 kb region between single nucleotide polymorphisms PERL0098471 and PERL0101839. A survey of the expression pattern of the 60 genes mapped in the marker region using AtGenExpress microarray data (http://www.arabidopsis.org/) found that *At1g33430* was expressed specifically in young flower buds at floral developmental stages **9** to **11** (as defined by Smyth et al.,

1990). These stages coincide with the development of the exine in microspores. Mutant alleles of this gene (*upex1*, *upex2*, SALK_091466, SAIL_544_C02) have previously been shown to have an uneven pattern of exine, which is also thin and composed of a very short baculae and overdeveloped tectum (Dobritsa et al., 2011). In addition, it was also reported that some regions of the exine of *upex* mutants partly lacked reticulate structure, being smooth with small lacunae; that their exine dissociated easily from the pollen surface; and that pollen grains were sticky (Dobritsa et al., 2011). These observations were similar and mostly consistent with our observations of *kns4-1* (Suzuki et al., 2008; Fig. 1, A–F), although we did detect subtle differences, such as the entire surface of *kns4* pollen grains being covered with reticulated exine to which pieces of debris clung (Fig. 1D), rather than a complete lack of exine. In this article, we use the term "lacunae" as the holes within the tectum (including the space directly beneath the tectum hole). When referring to the whole space under the tectum, including lacunae and gaps between neighboring baculae, we use the term "exine cavities". The lacunae of *kns4-1* were smaller and shallower, while their density was almost similar to that of wild type (compare Fig. 1, C and F). Taken together, these data suggested that *At1g33430* was a likely candidate to contain the causative mutation of *kns4-1*. The *kns4-1* mutant was shown to possess a G to A substitution in the fifth coding exon of *At1g33430*. This caused a change in the 276th codon from a Trp residue to a stop codon in the corresponding protein (Fig. 1G).

To validate that the genetic lesion in *At1g33430* leads to the pollen phenotype, the two aforementioned T-DNA lines (SALK_091466 and SAIL_544_C02, here designated *kns4-2* and *kns4-3*, respectively) were obtained that had insertions present either in the noncoding exon or the fourth exon, respectively (Fig. 1G). Both lines showed pollen phenotypes indistinguishable from those observed in *kns4-1*, namely a thin exine with a poorly reticulate tectum and considerable debris adhered to the pollen grain surface (Fig. 1, H–J).

To further confirm that the phenotypes observed in *kns4-1* mutants were due to a loss of *At1g33430* function, a complementation experiment was performed by generating a construct containing the wild-type coding sequence of *At1g33430* downstream of its own promoter (defined as 2006 bp upstream of the first Met, designated *ProKNS4:KNS4*) that was transformed into *kns4-1* mutant plants. The aberrant pollen phenotype was completely restored in all 17 individual T1 transformants (Fig. 1K). Taken together, we conclude that the phenotypes observed in *kns4-1* mutants are due to the loss of *At1g33430* function and that *kns4* and *upex* mutants (Dobritsa et al., 2011; Li et al., 2017) are synonymous.

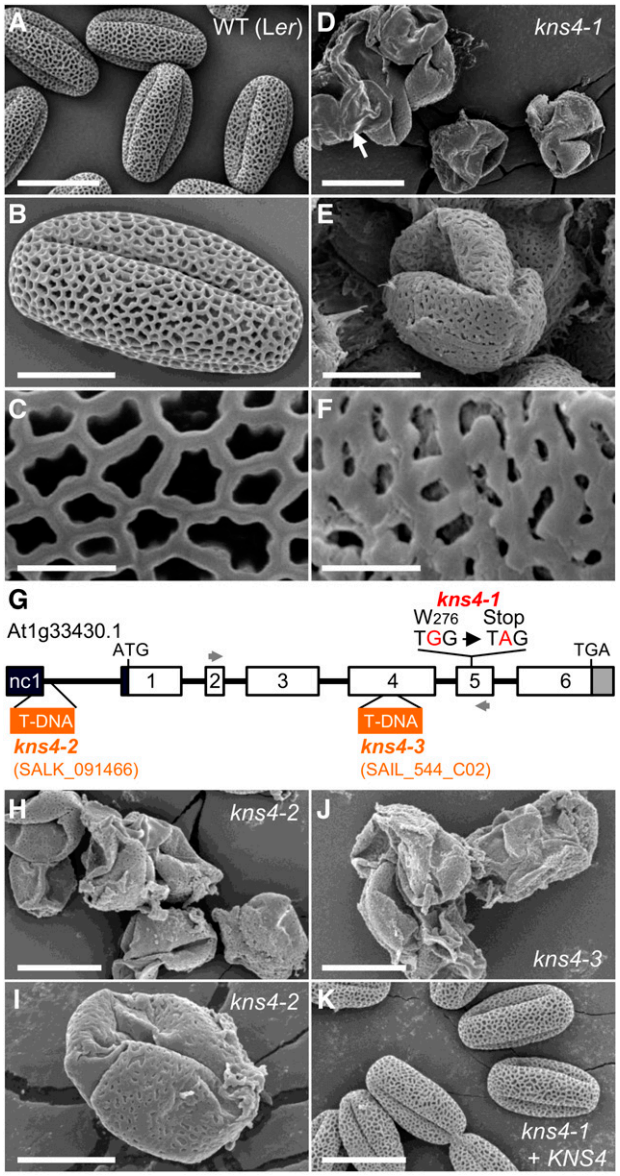

Figure 1. Pollen phenotypes of *kns4* mutants. A to F, Surface view of wild-type (L*er*; A–C) and *kns4-1* (D–F) pollen grains by SEM. Arrow in D indicates cell wall debris adhered to pollen grains. G, Schematic structure of *At1g33430*/*KNS4*. The shorter splice variant, *At1g33430.1*, is depicted, as only this form is detected in flower buds. Rectangles represent exons [noncoding exon 1 (nc1) and coding exons 1 to 6], and coding region and 5′ and 3′ UTRs are indicated with white, black, and gray, respectively. The thick black line represents noncoding sequence/introns. The positions of point mutation (*kns4-1*) and T-DNA insertions (*kns4-2* and *kns4-3*) as well as the SALK and SAIL line numbers are indicated. Gray arrows represent the position of primers used in the RT-PCR experiment shown in Fig. 4A. H to J, Surface view of *kns4-2* (H and I) and *kns4-3* (J) pollen grains by SEM. K, Rescued pollen phenotype of the *kns4-1* mutant after transformation with the *ProKNS4:KNS4* construct. Scale bars = 20 μm in (A, D, H, J, and K), 10 μm in (B, E, and I), and 2 μm in (C and F).

KNS4 Is Required for Separation of PMCs and Microspores in Anthers

To identify the initial defect in pollen development of *kns4* mutants, sections of resin-embedded *kns4-2* anthers were prepared at several floral bud developmental stages (stages **8** to **12**; as defined by Smyth et al., 1990) and counterstained with toluidine blue for visualization. Because stage **12** is rather long

(approximately 48 h), we divided this stage into a further three substages: **12E** (until the petals reach the style), **12M** (until anthers begin to turn yellow), and **12L** (thereafter). Furthermore, because microspores drastically change their morphology during stage **9**, we also divided this stage into three substages: **9E**, **9M**, and **9L**. For clarity, the morphological microspore/pollen development phenotype at each of these floral developmental stages is defined as follows: stage **8** (pollen mother cell [PMC] before initiation of callosic wall formation), stage **9E** (PMC surrounded by the callosic wall), stage **9M** (tetrad), stage **9L** (newborn unicellular microspore), stage **10/11** (unicellular), stage **12E** (unicellular to bicellular), stage **12M** (bicellular to tricellular), and stage **12L** (tricellular).

At stage **8** (PMC), all the PMCs were tightly adhered, either to each other or to tapetal cells and no obvious morphological differences were observed between wild type and *kns4* mutants (compare Fig. 2, A and G, respectively). The first sign of developmental abnormality in *kns4* mutants appeared in stage **9E** (PMC), when callosic wall formation had been initiated. At this stage, the wild-type PMCs began to separate from each other and from tapetal cells, whereas in the *kns4* mutant PMCs remained adherent and tapetal cells were slightly vacuolated and swollen (compare Fig. 2, B and H, respectively). Moreover, the protoplast of the wild-type PMCs was often detached from the primary cell wall, although this is likely to be a sample preparation artifact frequently observed during this developmental stage in wild type (Quilichini et al., 2014). Interestingly, this was never observed in mutant PMCs, perhaps indicating some structural differences in connectivity between the plasma membrane-cell wall interface between wild type and mutants. At stage **9M** (tetrad), when the callosic wall of tetrads was clearly observed to stain strongly with toluidine blue, wild-type tetrads were separated and dispersed in anther locules, whereas the *kns4* tetrads remained attached to tapetal cells and appeared to adhere to each other (compare Fig. 2, C and I, respectively). In the *kns4* mutant the tapetal layer is thicker relative to wild type, resulting in a compression of the tetrads.

After the dissolution of the callosic wall at stage **9L**, spherical microspores were scattered in anther locules at stage **10/11** (unicellular) in wild type, but deformed microspores of the mutant did not separate from each other and filled the locules (compare Fig. 2, D and J, respectively). Interestingly, the tapetal cells in *kns4* mutants appeared to be vacuolated compared with the wild type. Microspores of both wild type and *kns4* mutants gradually grew larger during stage **12E**, although their morphology was similar to the previous stage. At stage **12M** (bicellular), most of the mutant microspores were still in contact with each other and many seemed tightly adhered to tapetal cells, even though a small space appeared in the center of each locule (compare Fig. 2, E and K, respectively). Strikingly, the vacuolated tapetal cell phenotype observed in the *kns4* mutants at stage **10/11** appeared to be more obvious, particularly when compared with the wild type (compare Fig. 2, D and E with Fig. 2, J and K, respectively). At stage **12L** (tricellular) in wild type, when tricellular mature pollen grains were developed, the tapetal cells disappear and only pollen grains can be observed (Fig. 2F). However, in *kns4* locules, debris that stained weakly with toluidine blue remained attached to the surface of pollen grains (Fig. 2L). In these *kns4* locules, many pollen grains were found to adhere to each other and to the surface of the anther cell wall (endothecium), presumably due to the presence of the debris. Some collapsed pollen grains were also observed (Fig. 2L). These observations suggest that pollen adhesion and debris formation in the *kns4* mutant is a consequence of the defect in separation of the PMC at stage **9E**.

KNS4 Is Required for Sporopollenin Deposition and Exine Development

Exine development in *kns4* mutants was further investigated by transmission electron microscopy (TEM). In the tetrads of wild-type stage **9M** anthers, a matrix of primexine appeared as a layer between the plasma membrane of the microspore and the callosic wall, in which the development of the exine framework consisting of the probaculae and tectum is initiated (Fig. 2M). The primexine is thinner and consequently the probaculae are shorter in the *kns4* mutant than those in wild type, whereas tectum development was essentially normal in the mutant (Fig. 2Q). These results indicate that the characteristic exine phenotype in the *kns4* mutant is related to an abnormality of thin primexine in the tetrads.

At stage **10/11**, mutant microspores clumped together, whereas wild-type microspores were already separated, with distinct exine walls (compare Fig. 2, R and N, respectively). By the end of stage **12E**, sporopollenin supplied by tapetal cells settles onto the surface of each microspore and exine development is nearly complete in wild type (Fig. 2O). In contrast, exine walls in the *kns4* mutant microspores appeared compacted and tectum and baculae structures were not well defined (Fig. 2S). A considerable amount of sporopollenin secreted by *kns4* mutant tapetal cells was deposited both on the surface of microspores and tapetal cells adjacent to the microspores, which appeared to result in the adhesion of microspores to tapetal cell walls (Fig. 2, R and S). Electron-dense particles, presumably containing sporopollenin, were also deposited on the walls separating adjacent tapetal cells (Fig. 2R). Interestingly, exine structures of two adjacent microspores were always separated and never fused (Fig. 2, R and T). At stage **12L** in wild type, the tapetal cells have already collapsed and osmiophilic materials have filled the exine cavities of tricellular pollen grains to form the pollen coat (Fig. 2P). Pollen coat formation was similarly observed on the surface of *kns4* pollen grains, although the amount of material was very low compared to wild type due to the short baculae length (Fig. 2U).

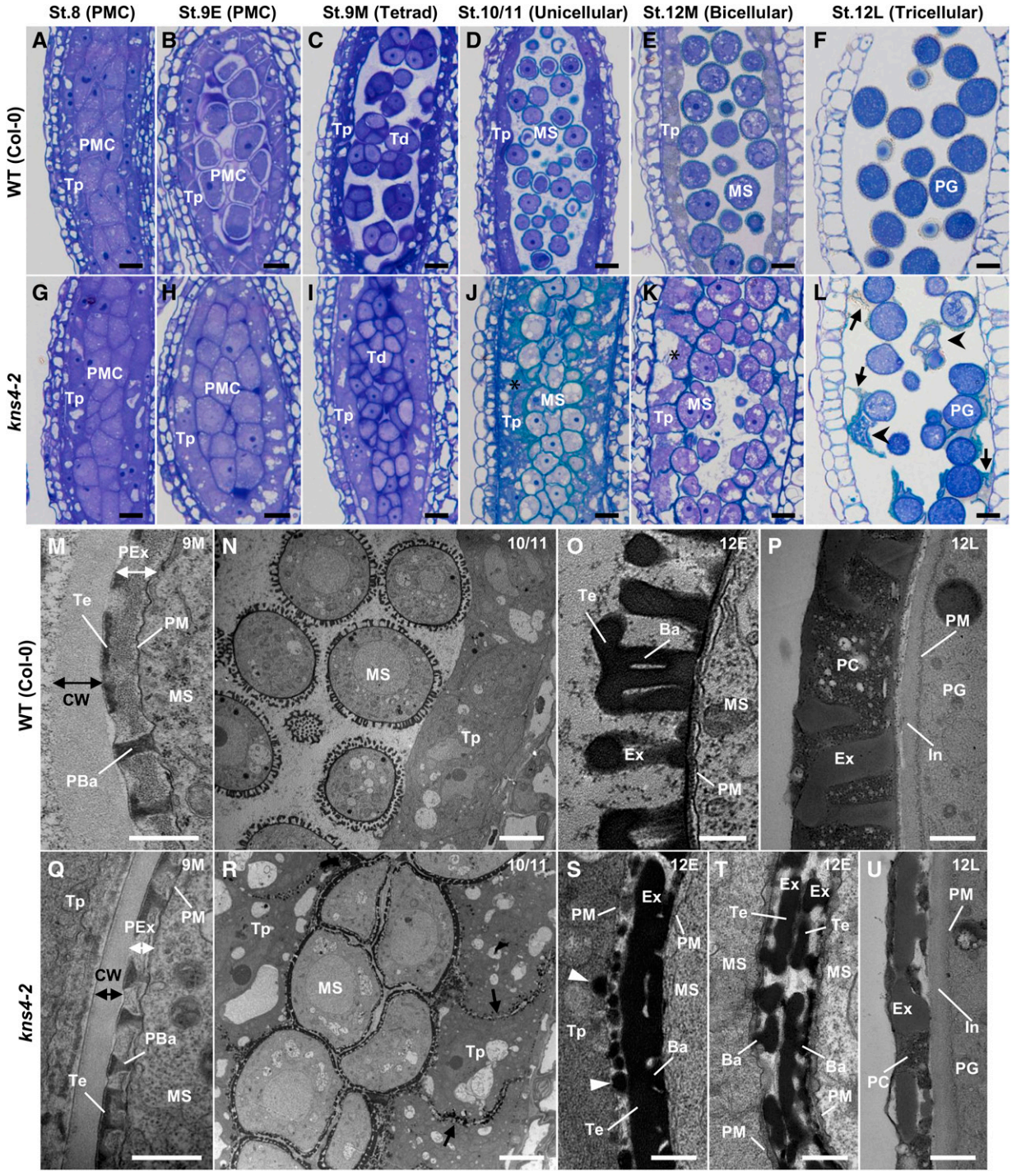

Figure 2. Light and TEM micrographs reveal defects in pollen development in *kns4-2* mutants. A to L, Light micrographs of longitudinal sections of resin-embedded anthers of wild-type (Col-0; A–F) and *kns4-2* (G–L) plants stained with toluidine blue. Developmental stages (stages **8L** to **12L**) of anthers are indicated along with the developmental stage of pollen development in parentheses. Asterisks in (J) and (K) indicate swollen and vacuolated tapetal cells in the mutant. Arrows and arrowheads in (L) indicate cell wall debris and crushed pollen grains, respectively. M to U, TEM images of wild-type (Col-0; M to P) and *kns4-2* (Q to U) anthers. M and Q, Primexine layers and developing exine in tetrads at stage **9M**. (N, O, R, S, and T), Longitudinal section of stage **12E** anthers containing unicellular microspores. (P) and (U), Exine and pollen coat of pollen grains (tricellular stage) at stage **12L**. Arrows in (R) show walls between tapetal cells. Arrowheads in (S) show granules containing sporopollenin deposited on the surface of tapetal cell wall. Ba, Bacula; CW, callosic wall; Ex, exine; In, intine; MS, microspore; PBa, probacula; PC, pollen coat; PG, pollen grain; PM, plasma membrane; PMC, pollen mother cell; Td, tetrad; Te, tectum; Tp, tapetal cell. Scale bars = 10 μm in (A–L), 5 μm in (N and R), and 0.5 μm in (M, O, P, Q, S, T, and U).

Exine development in wild type and *kns4* was observed and exine thickness measured by use of optical sections of isolated microspores and pollen grains (Supplemental Fig. S1). The thickness of wild-type exine gradually increased from stage **9L** to stage **10/11** and reached a peak at stage **12E**. Thereafter, it decreased slightly until the mature pollen grain stage in open flowers. The exine of *kns4* microspores was 24% thinner than wild-type exine at stage **9L**, and decreased to less than 50% at stage **12E** and later stages. These results suggested that *KNS4* function is also required for exine thickening from stages **9L** through to **12E**, which is consistent with the expression pattern of *KNS4* (described below).

To examine the origin of the debris adhering to the *kns4* pollen grains, cross sections of paraffin-embedded anthers were prepared, stained with calcofluor white, and viewed under UV excitation (Fig. 3, A–F). In wild-type anthers at stage **9L**, most cell walls fluoresced blueish-white, whereas tapetal cells and microspores showed weak yellow fluorescence (Fig. 3A), suggesting that the walls of tapetal cells and early unicellular microspores did not contain much cellulose or callose. The yellow autofluorescence of polymerizing sporopollenin appeared on the developing exine and reached maximal brightness at stage **12E** (Fig. 3B). When the anthers reached stage **12M**, intine appeared on pollen grains and fluoresced blueish-white, while yellow exine autofluorescence became weaker (Fig. 3C). In the mutant stage **12E** anthers, the yellow autofluorescence was observed not only on the developing exine but also, and more strongly, on the boundaries between tapetal cells and microspores (white arrows) and the walls separating adjacent tapetal cells (red arrows; Fig. 3D). This is consistent with the abnormal sporopollenin deposition in these walls observed by TEM (Fig. 2, R and S). The yellow fluorescent walls in *kns4-2* were still observed at stage **12M** (Fig. 3E), and even after anther dehiscence (Fig. 3F). It therefore appears that tapetal cell walls were not completely degraded when these cells collapsed, and remained adhered to the *kns4* microspore surface as pollen grain development was completed. Thus, we suggest that the material adhering to *kns4* pollen grains is not dissociated exine, but rather remnants of tapetal cell walls onto which sporopollenin was deposited (Fig. 3F).

While neighboring *kns4* mutant pollen grains were never observed to fuse (Fig. 2T), mutant pollen grains did form clumps that could be squeezed out from anthers (Fig. 3G). This observation implies the existence of adherent material(s) that connect the microspores. During tetrad stage (stage **9M**), microspores are separated by walls rich in callose, which can be visualized by confocal laser scanning microscopy (CLSM) using the aniline blue fluorochrome. No staining differences were readily observed when comparing wild type to *kns4* mutants (compare Fig. 3, I and K). However, at stage **12E**, when the callosic walls are completely degraded in wild type and hence the aniline blue signal is absent, *kns4* microspores continued to show aniline blue signal between the microspores within the tetrad (compare Fig. 3, J and L). Aniline blue fluorescence was also detected in the walls of *kns4* microspore clumps squeezed from mature anthers (Fig. 3H). These results suggest that the remnant callose in the walls between microspores prevents the developing exine from fusing in the *kns4* mutant.

Expression Analysis of *KNS4*

Reverse transcription PCR (RT-PCR) analysis of a variety of tissue types revealed that *KNS4* expression (mRNA) is only detected in the inflorescence apices containing shoot apical meristems and flower buds up to stage **12L** (Fig. 4A). This observation is consistent with transcript levels reported in AtGenExpress microarray datasets (http://www.arabidopsis.org/). No *KNS4* transcripts were detected in either *kns4-2* or *kns4-3* inflorescence apices (Fig. 4A), indicating that both T-DNA insertions disrupted gene function.

To more specifically determine the tissues/organs where *KNS4* is expressed, the *KNS4* promoter was separately fused to β-glucuronidase (GUS) and GFP, and the reporter constructs introduced into wild-type Arabidopsis plants. In all 14 individual T1 *ProKNS4:GUS* transformants, the GUS signal was specifically detected in anthers with strongest staining in young flower buds and reduced signal in older open flowers (Fig. 4B. No signal was observed in any other organs including leaves, stems, roots, and fruits, consistent with the RT-PCR analysis and the public microarray datasets (Fig. 4A). The same result was obtained for all 10 individual T1 transformants carrying the *ProKNS4:GFP* transgene (Fig. 4, C–F. Imaging revealed that the GFP fluorescence was specifically detected in anthers ranging from stages **8** through to **10/11**, with the strongest expression at stage **9L** (Fig. 4, C–F).

We also examined *KNS4* mRNA levels in anthers by quantitative RT-PCR (qRT-PCR; Fig. 4G). *KNS4* transcript was detected from stages **8** through to **12E**, declining in stage **12M** and **12L** along with the degeneration of tapetal cells (Fig. 4G). These results indicated that *KNS4* might have a constitutive function in tapetal cells. It should be noted that the expression of *ProKNS4:GFP* did not reflect the accumulation of *KNS4* mRNA at stages **10/11** and **12E**, possibly due to the differential stabilities of mRNAs.

To more accurately define the location of *KNS4* transcripts, we performed in situ hybridization of anthers from stage **8** through to stage **10/11**. While the sense probe resulted in little signal (Fig. 4, M–Q), the antisense probe produced strong signals in tapetal cells throughout these stages, with the strongest labeling detected at stage **9** (Fig. 4, H–L). The relatively high background signal by the antisense probe in young anthers possibly reflects weak *KNS4* expression in tissues other than tapetum, which has been suggested in a previous study (Peiffer et al., 2008).

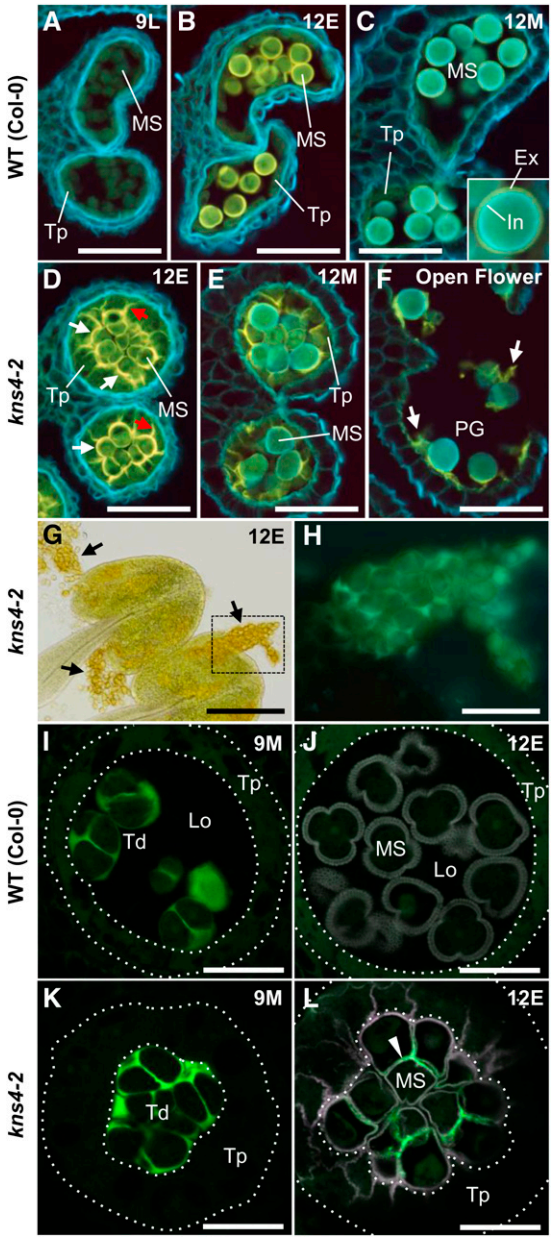

Figure 3. Abnormal sporopollenin deposition and delayed callose degradation in *kns4-2*. A to F, Calcofluor white staining of anther cross sections in wild type (Col-0; A to C), and *kns4-2* (D–F) observed by fluorescence microscopy. Sections of stage **9L** (newborn unicellular; A), stage **12E** (unicellular; B and D), stage **12M** (bicellular; C and E), and open flower (stage **14**, tricellular; F) are shown. Cell walls containing cellulose and callose are stained whitish blue, and autofluorescence of sporopollenin is yellow. White and red arrows in (D) indicate boundary between tapetal cells and microspores and the walls separating adjacent tapetal cells, respectively. White arrows in (F) indicate tapetal wall remnant onto which sporopollenin is deposited. G and H, Aggregates of microspores (black arrows) squeezed out from *kns4-2* anthers at stage **12E** were observed with transmitted light (G) and fluorescence microscopy (H) after aniline blue staining; (H) shows the framed area in (G). I to L, Aniline blue staining of anther cross sections in wild-type (Col-0; I and J) and *kns4-2* (K and L) observed by CLSM. Stages are **9M** (tetrad; I and K) and **12E** (unicellular; J and L). Green and magenta channels show fluorescence of aniline blue and sporopollenin autofluorescence, respectively. Dotted lines indicate the position of the tapetum. Arrowhead in (L) indicates callose in walls that remained in late unicellular stage. Ex, Exine; In, intine; Lo, locular space; MS, microspore; PG, pollen grain; Td, tetrad; Tp, tapetal cell. Scale bars = 50 μm in (A– F) and H, 200 μm in (G), 20 μm in (I–L).

Enzymatic Activity of KNS4

KNS4 is predicted to encode a β-(1,3)-galactosyltransferase (GalT) that belongs to GT family 31 (CAZy; http://www.cazy.org; Strasser et al., 2007; Qu et al., 2008; Egelund et al., 2011). Among the members of this family, *At1g77810*, one of the closest homologs of *KNS4*, has been shown to encode a β-(1,3)-GalT (Qu et al., 2008). An enzyme with this activity is required for the biosynthesis of the β-(1,3)-galactan core structure of type II AGs, the glycan moieties that decorate AGPs (Ellis et al., 2010; Showalter and Basu 2016), as well as the type II AG side chains on RG-I (Mohnen, 2008). Furthermore, it was recently reported that the gene product of another close homolog, AtGALT31A (At1g32930), possesses β-(1,6)-GalT activity, which is also required for the formation of side chains in type II AGs (Geshi et al., 2013). Thus, it was thought that KNS4 may have a similar GalT enzymatic activity.

To examine this possibility, the full-length *KNS4* coding sequence was transiently expressed in *Nicotiana* leaves. As a negative control, the yellow fluorescent protein VENUS was also transiently expressed. Microsomal membrane (MM) fractions prepared from leaves 4 d post-infiltration were used as the enzyme source in biochemical activity assays using fluorescent β-Gal-NBD as the acceptor (McGill and Williams, 2009; Fig. 5). When MMs prepared from the control plants were assayed in the presence of UDP-Gal, the reversed phase-HPLC profile was indistinguishable from the β-Gal-NBD standard, indicating the absence of detectable endogenous enzyme activity under these assay conditions (Fig. 5A). In contrast, when MMs derived from *KNS4*-expressing leaves were assayed under the same conditions, a series of new peaks were observed with R_t of 9.6 min (Peak 2), 8.7 min (Peak 3), and 8.1 min (Peak 4; Fig. 5B). The donor specificity was restricted to UDP-Gal as none of the other UDP-sugar donors tested (UDP-Glc, UDP-Ara*p*, and UDP-Xyl) resulted in the formation of product using β-Gal-NBD as the acceptor (Supplemental Fig. S2).

To determine the nature of the glycosidic linkage(s) in the NBD-labeled products formed by the KNS4 MM preparation, the oligosaccharide products were digested with SGalase1, an exo-β-(1,3)-D-galactanase (CAZy GH family 43) that has been shown to specifically cleave the β-(1,3)-D-galactan backbone of AGPs (Ling et al., 2012; Fig. 5C). SGalase1 digestion resulted in the hydrolysis of all the reaction products to β-Gal-NBD (R_t is approximately 11.5 min). A commercial *Escherichia coli* β-galactosidase, which also digests the Gal-NBD bond, hydrolyzed these same oligosaccharides in KNS4

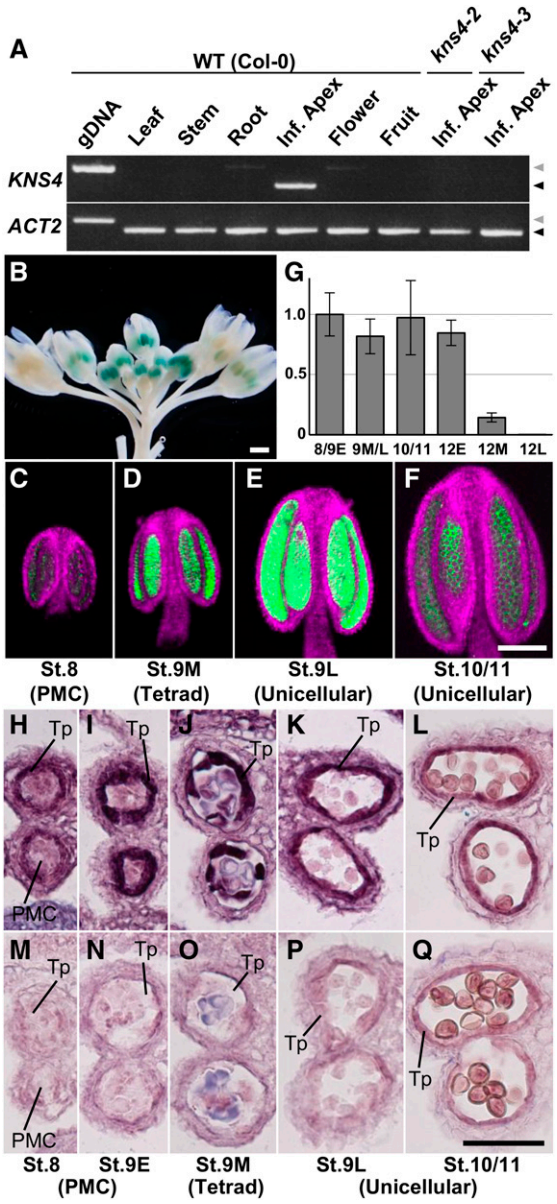

Figure 4. *KNS4* is specifically expressed in tapetal cells in young anthers. A, RT-PCR analysis of *KNS4* using RNA extracted from rosette leaves, inflorescence stems, roots, inflorescence apices, open flowers, and fruits (siliques) of wild-type Arabidopsis (Col-0), and inflorescence apices of *kns4-2* and *kns4-3* mutants. Leftmost lane shows the PCR product amplified from Col-0 genomic DNA (gDNA) with the same primer set. *ACT2* was used as a control. Black and gray triangles indicate cDNA- and gDNA-derived bands, respectively. B, *ProKNS4-GUS* expression in flower buds. C to F, *ProKNS4-GFP* expression in anthers from stages **8** to **10/11** observed by CLSM. Green and magenta channels show GFP signal and chlorophyll autofluorescence, respectively. G, Expression levels of *KNS4* in anthers at various flower developmental stages (stages **8** and **9E**, **9M** and **9L**, **10/11**, **12E**, **12M**, and **12L**) measured by qRT-PCR. Bars show relative average expression values (stage **8/9E** = 1) of triplicate samples ± SD. H to Q, In situ hybridization using either an antisense (H–L) or sense (M–Q) probe for *KNS4*. Cross sections of paraffin-embedded anthers from stages **8** to **10/11** were examined. Scale bars = 1 mm in B, 100 μm in (C–F), and 50 μm in (H–Q).

MM preparations to NBD (R_t is approximately 17.0 min; Fig. 5D). Analysis of the assay products by electrospray ionization (ESI)-MS/MS revealed the presence of the protonated pseudo-molecular ions [M+H] of m/z: 552.2, 714.3, 876.3, 1038.4, and 1200.4 corresponding to β-Gal-NBD, Gal_2-NBD, Gal_3-NBD, Gal_4-NBD, and Gal_5-NBD, respectively (Fig. 5E). The mass difference between each of the pseudo-molecular ions is 162 dalton, indicating a hexose series (Fig. 5E). Thus, from the combined linkage-specific enzyme digestions and the MS data we can conclude that KNS4 is a β-(1,3)-GalT likely to play a role in type II AG glycan biosynthesis on either AGPs or RG-I.

Distribution of AGP Epitopes in Developing Anthers

To investigate the impact of the *kns4* mutant on the accumulation of AGPs in anthers, cross sections of young flower buds up to stage **12M** were labeled with the JIM8 antibody that recognizes the AG epitope on AGPs (Pennell et al., 1991; Fig. 6, A–H). At stage **8**, JIM8 labeling was observed in the cell walls surrounding the PMCs in both wild-type and *kns4* mutant anthers (Fig. 6, A and E). Bright, punctate signals were observed within the cytoplasm of the PMCs, tapetal cells, middle layer cells, and endothecial cells, which likely corresponds to the endoplasmic reticulum/Golgi apparatus as they are known to be the intracellular sites of AGP biosynthesis. At stage **9M**, JIM8 strongly labeled the outer surface (primary walls) of wild-type tetrads and the tapetal walls facing the locule (Fig. 6B). JIM8-labeled signal was also observed in primexine in tetrads (inset in Fig. 6B). In *kns4* mutants, signal could still be detected, but was much weaker (Fig. 6F). At stage **12E**, the cavities of the developing exine and walls of the tapetal cells were labeled in wild type, but only weak punctate signals were observed in the walls of *kns4* tapetal cells (compare Fig. 6, C and G, respectively). By stage **12M** in wild type, the JIM8 signal in the exine cavities and on the locular surface of tapetal walls had decreased (Fig. 6D). The signal in *kns4* was similarly weaker at the same stage (Fig. 6H). In contrast, walls and cytoplasm of endothecial cells in both wild type and *kns4* were strongly labeled by JIM8 throughout anther development.

Distinct immunolabeling results were obtained using another anti-AGP antibody, MAC204 (Bradley et al., 1988). This antibody specifically labeled tapetal walls and developing exine cavities in wild type (Fig. 6, I–L). In contrast to JIM8, MAC204 only faintly labeled the primary walls of PMCs and tetrads, and no labeling was observed in the endothecium. The signal in the tapetal walls at stage **12E** was very weak and restricted to the locular surface, whereas fluorescence in exine cavities was bright and remained in stage **12M**. In the *kns4* mutant, the signals on tapetal cell walls appeared similar to wild type at early developmental stages (stage **8**), but decreased in later stages (stage **9M** and beyond) with very weak labeling observed in exine cavities (Fig. 6, M–P).

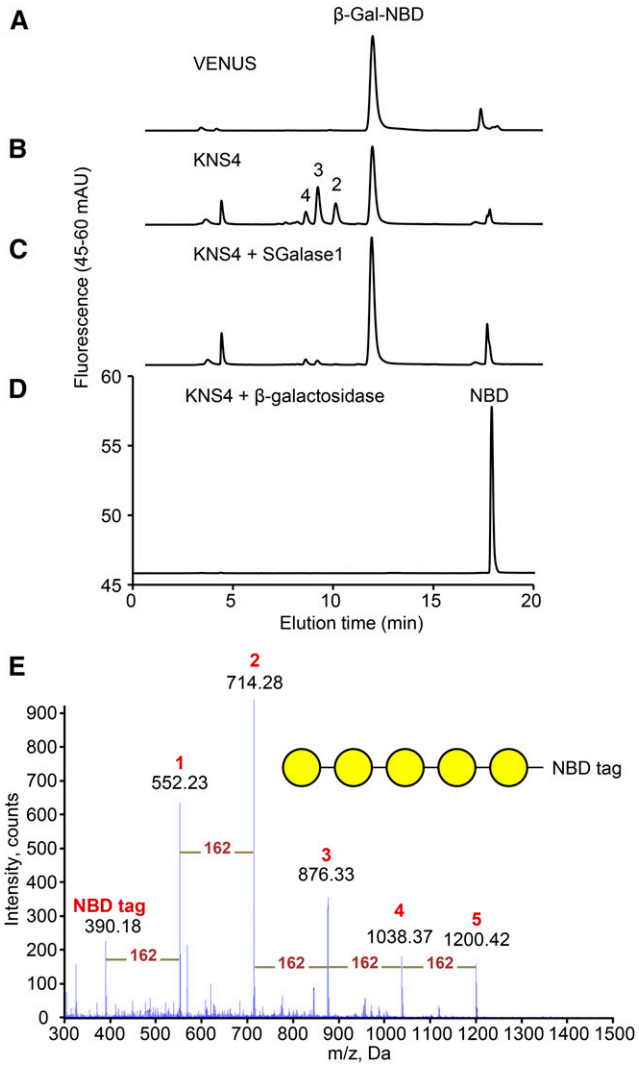

Figure 5. Enzymatic activity of heterologously expressed KNS4 in microsomal membranes from *Nicotiana* leaf. A and B, RP-HPLC profiles of GalT enzyme assay products with KNS4-expressing MMs in the reaction mixture (B) and control experiment with VENUS-expressing MMs (A). Numbers above peaks indicate the number of Gal residues. C and D, Treatment of the KNS4 reaction products with either SGalase1 (C) or β-galactosidase (D). E, ESI-MS full scan spectrum of KNS4 GalT enzyme assay products. Peaks corresponding to β-$Gal_{1\text{-}5}$-NBD are labeled 1 to 5, respectively. Yellow circles represent Gal residues.

Given the demonstrated β-(1,3)-GalT activity of KNS4 (Fig. 5), the reduced labeling with two AGP antibodies (Fig. 6) and the loss of exine thickening observed in *kns4* mutants (Supplemental Fig. S1), we hypothesized that AGPs play a critical role in exine development. Thus, to test whether the *kns4* mutant phenotype is due to a loss of AGPs, we examined the localization of AGP epitopes using the MAC204 antibody specifically in relation to exine development at stages **9L** to **12E** in isolated microspores. In wild type at stage **9L**, a strong signal was observed surrounding the microspores just released from tetrads (Fig. 7A). Under higher magnification, we found that a layer of AGPs overlays the developing exine (the position of the AGP layer in relation to the exine is indicated by blue and white arrowheads in Fig. 7G) and localized on the top of baculae (yellow arrowhead in Fig. 7G). An optical section near the surface of the microspore revealed a reticulate pattern of MAC204 labeling (Fig. 7H), indicating that at this developmental stage the AGPs formed a reticulate structure overlaying the tectum. At stage **10/11**, while the exine gradually thickened, most AGP still overlayed the tectum but some began to be redistributed into the exine cavities (Fig. 7B). At stage **12E**, when the exine reaches its maximum thickness in wild type (Supplemental Fig. S1), MAC204 signal was also strongest (Fig. 7C). AGP labeling was reduced at the exine surface but appeared in the exine cavities (in the space between baculae (yellow arrowheads in Fig. 7I)). Tangential optical sections showed the non-uniform distribution of AGPs in the cavities of the reticulate exine, specifically they were absent from both baculae and lacunae (white and red arrowheads, respectively in Fig. 7J). In *kns4* microspores, MAC204 labeling in the exine was reduced across all stages, being either absent (Fig. 7D) or localized on only a part of the microspore surface (Fig. 7, E and F). The redistribution of signal from the outer layer at stage **9L** to within the exine cavities at stage **12E** was not as obvious in the mutant compared to wild type (compare Fig.7, K–N to Fig. 7, G–J, respectively). These results suggest an association between AGP deposition and exine formation and that the synthesis of AGPs is dependent on the function of *KNS4*.

To further validate that the loss of *KNS4* function leads to a reduction in AGPs in developing microspores, we used the AGP-specific β-Glc Yariv reagent to stain stage **12M** microspores of both wild-type (Fig. 8B) and *kns4* mutants (Fig. 8, E and H). AGPs were detected in the wild-type exine as indicated by orange/red staining of the microspore surface while minimal staining was observed in the wall of *kns4* microspores. Control experiments using α-Gal Yariv reagent showed similar levels of background staining in wild-type (Fig. 8A) and *kns4* mutant (Fig. 8, D and G) microspores. The β-Glc Yariv staining is consistent with more AGPs being present on the surface of developing wild-type microspores compared with the *kns4-2* and *kns4-3* mutants.

Localization of AGPs in the exine cavities was examined in further detail by immuno-TEM using JIM8 and another AGP epitope antibody, JIM13 (Supplemental Fig. S3). In wild-type stage **12M** microspores, most JIM13 labeling was seen in the locular space, on the exine and in exine cavities, and at the base of exine (nexine layer; Supplemental Fig. S3, B and G). A sparse but similar labeling pattern was observed with JIM8 (Supplemental Fig. S3A). In *kns4* microspores, JIM8 and JIM13 labeling was generally similarly located, although more label was detected outside the exine (Supplemental Fig. S3, D, E, and G). Labeling of the sporopollenin granules was also seen (Supplemental Fig. S3E). Callose labeling was detected mainly in the nexine II layer in both the wild-type and *kns4* mutants (Supplemental Fig. S3, C and F, respectively), indicating no impact on the synthesis and deposition of this polysaccharide.

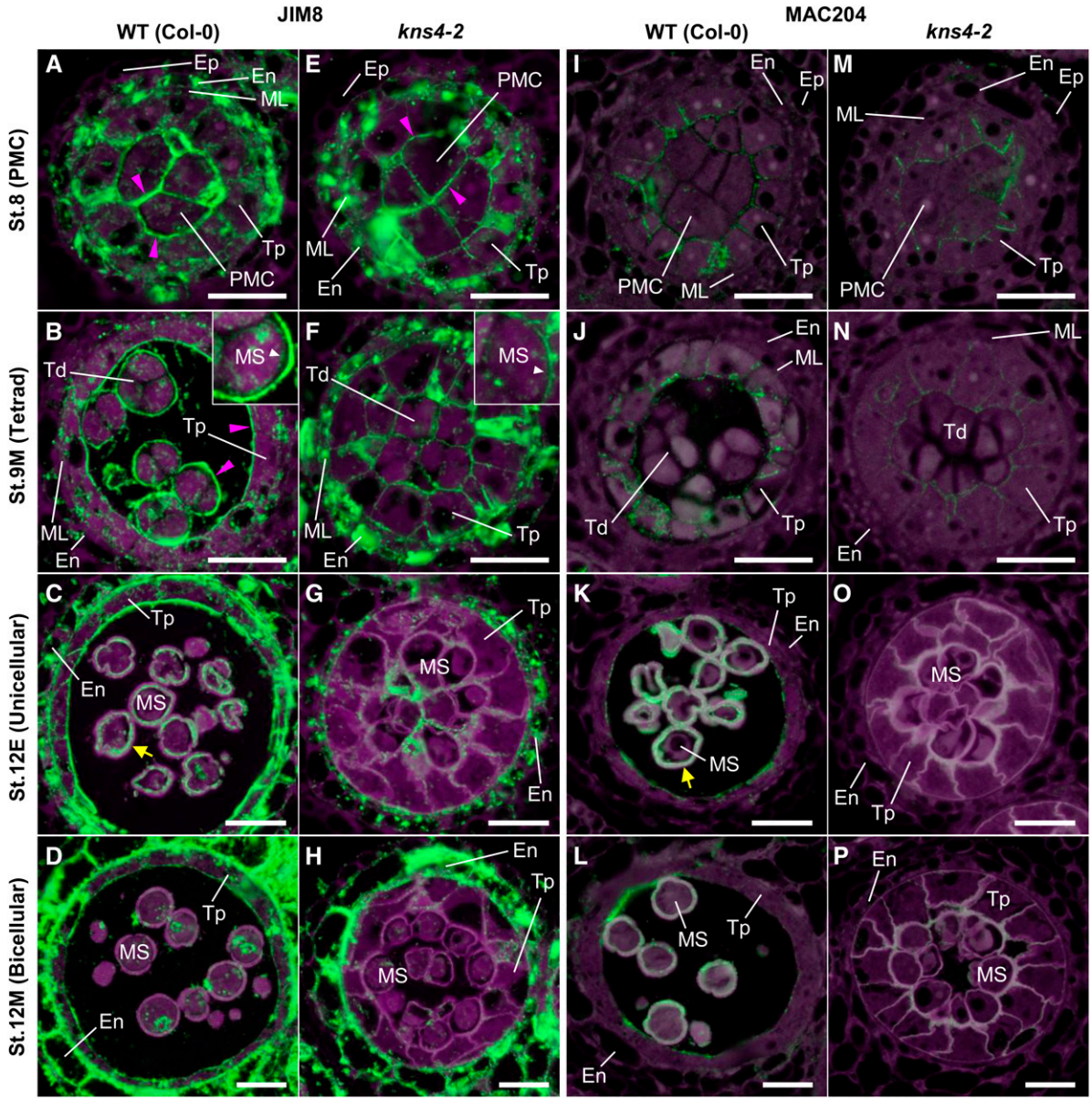

Figure 6. Distribution of JIM8- and MAC204-epitope labeling of AGPs in microsporocytes and microspores. Cross sections of resin-embedded anthers of wild type (Col-0; A–D and I–L) and *kns4-2* (E–H and M–P) from stages **8** to **12M** were incubated with the JIM8 (A–H) and the MAC204 (I–P) antibodies, and subsequently with Alexa Fluor 488-labeled secondary antibody. Fluorescence of Alexa Fluor 488 (green) and autofluorescence (magenta) were separately captured by epifluorescence microscopy and overlaid. Magenta arrowheads indicate the signal in the primary cell wall of the PMC, tetrad, and tapetal-cell walls facing the locule. Yellow arrow indicates the signal in the exine cavities. Insets in (B) and (F) are enlargements of a microspore in a tetrad. White arrowhead indicates the signal in primexine. En, Endothecium; Ep, epidermis; ML, middle layer cell; MS, microspore; PMC, pollen mother cell; Td, tetrad; Tp, tapetal cell. Bars = 20 μm.

Pectin and AGP Distribution Overlap in Developing Anthers

Pectins are known to be involved in cell-to-cell adhesion and cell separation in higher plants (for review, see Caffall and Mohnen, 2009). Pectins are generally composed of HGs, RG-I, and RG-II, and are synthesized in the GA; in the case of HG, the major type of pectin, as a highly methylesterified form that is then demethylesterified by pectin methylesterases after being deposited into the wall (Mohnen, 2008). Pectins are present on the surface of tetrads and defects in their degradation cause abnormal exine fusion (*quartet* phenotype; Rhee and Somerville, 1998). Moreover, pectins have been shown to be a component of primexine (Rhee and Somerville, 1998; Aouali et al., 2001; Majewska-Sawka et al., 2004). To test if the cell-to-cell adhesion

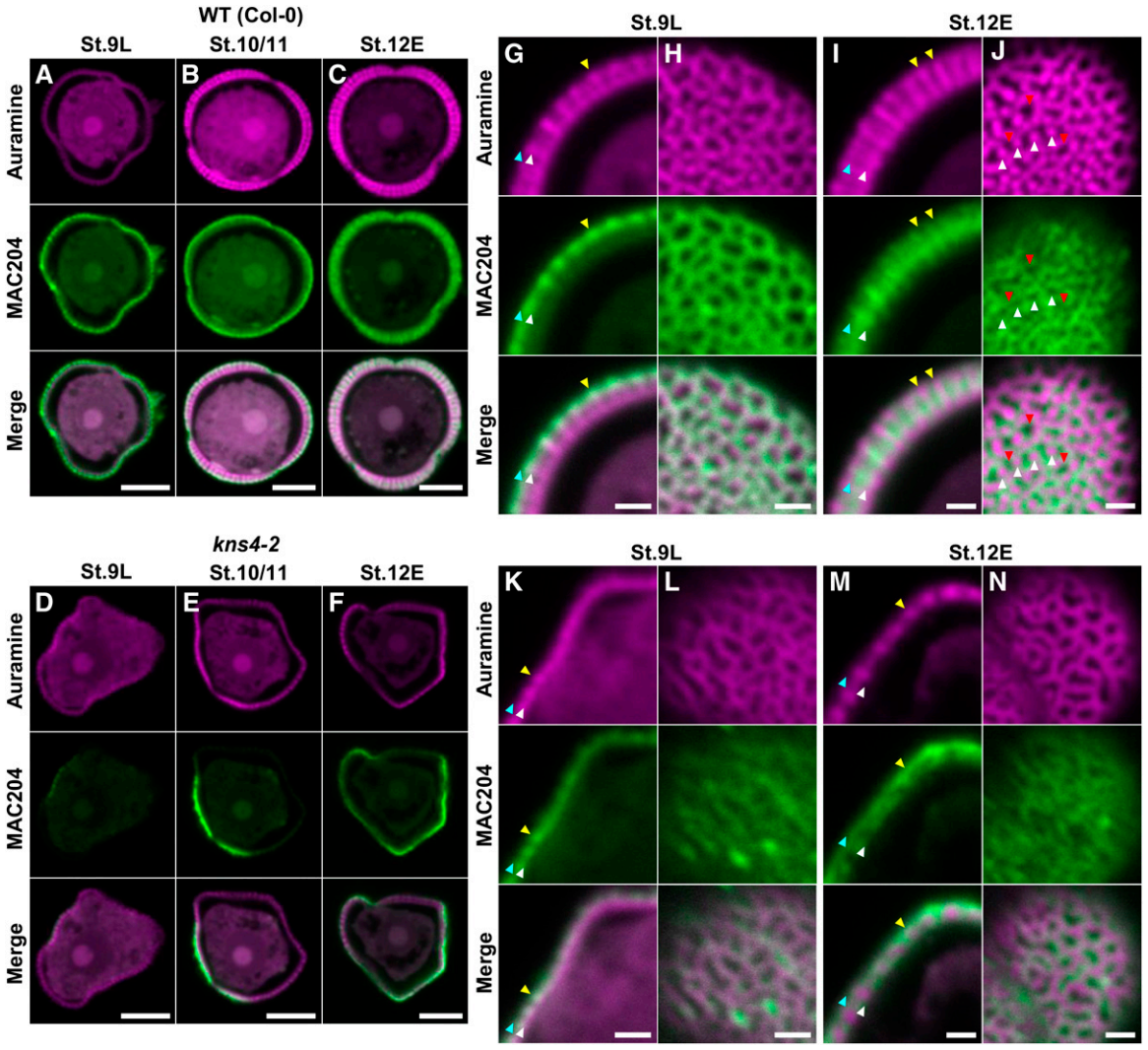

Figure 7. Distribution of MAC204-epitope labeling of AGPs on the surface of developing microspores. A to F, Median optical sections of wild type (Col-0; A–C) and *kns4-2* (D–F) microspores isolated from stages **9L**, **10/11**, and **12E** anthers after labeling with the MAC204 antibody and subsequently with Alexa Fluor 546-labeled secondary antibody. Exine was visualized by auramine O staining. Specimens were observed by CLSM in which magenta and green channels show fluorescence of auramine O and Alexa Fluor 546, respectively. G to N, Enlarged optical sections of wild-type (G–J) and *kns4-2* (K–N) microspores isolated from stages **9L** (G, H, K, and L) and **12E** (I, J, M, and N) anthers. (G, I, K, and M) are median optical sections of microspores showing the exine in longitudinal cross section. Blue, white, and yellow arrowheads indicate the top and bottom boundary of the AGP layer, and the top of representative bacula, respectively. (H, L, and N) are tangential optical sections almost at the microspore surface. J, Tangential optical section that transversely cuts baculae. White and red arrowheads indicate the position of representative baculae and lacunae, respectively. Bars = 5 μm in (A–F), and 1 μm in (G–N).

and thin exine phenotypes in *kns4* anthers were due to changes in the distribution of pectic polysaccharides and/or their methyl-esterification, two monoclonal antibodies, JIM7 and JIM5, recognizing highly methyl-esterified and less methylesterified pectins (HG), respectively (Knox et al., 1990), were used in labeling experiments.

In wild type at stage **8**, JIM7 strongly labeled the walls separating PMCs and tapetal cells (Fig. 9A). At stage **9M**, the primary walls of tetrads, which were detached from each other and from tapetal walls, were strongly labeled (Fig. 9B). After the degradation of the callosic walls, the labeling on the surface of microspores was visible (Fig. 9, C and D). A similar labeling pattern was detected in *kns4* mutants when compared to the wild type (compare Fig. 9, E–H to Fig. 9, A–D, respectively). In contrast, the distribution of JIM5 labeling (Fig. 9, I–P) was distinct from that of JIM7. Specifically, no signal was detected in the primary walls of the PMC (stage **8**) and tetrad (stage **9M**) in both wild type (Fig. 9, I and J, respectively) and *kns4* (Fig. 9, M and N, respectively). Note that the JIM5 images have higher

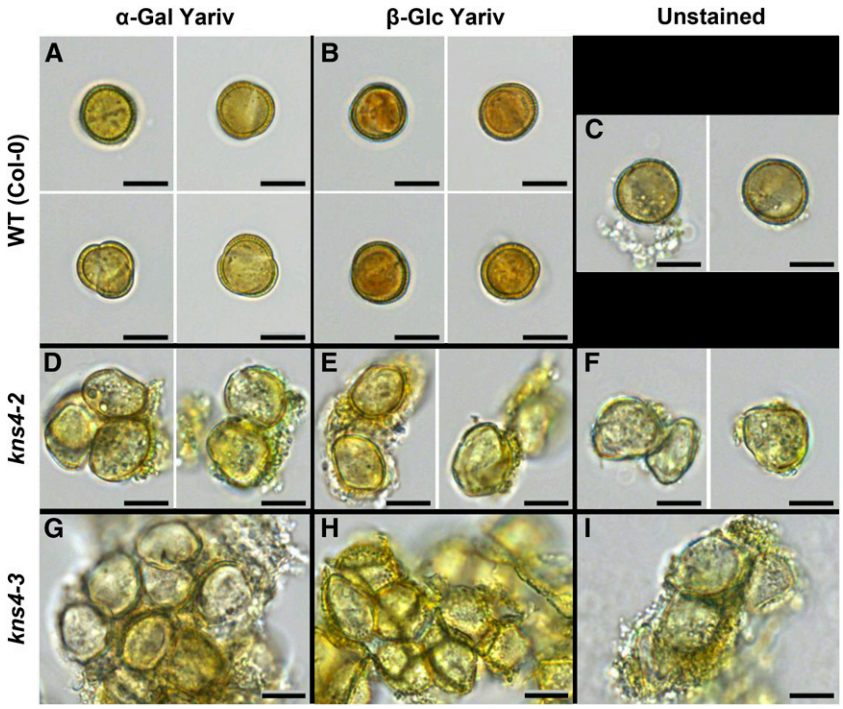

Figure 8. Yariv dye reagent staining of microspores (stage **12M**) isolated from flower buds of wild type and *kns4* mutants. Microspores from wild type (Col-0; A–C), *kns4-2* (D–F), and *kns4-3* (G–I) were independently stained either with α-Gal Yariv (A, D, and G), β-Glc Yariv (B, E, and H), or left unstained (C, F, and I) and viewed with light microscopy. Positive staining is observed as a reddish-orange color. Bars = 20 μm.

background signal in comparison to the JIM7 images (compare Fig. 9, I–P, and Fig. 9, A–H, respectively) because the signal was weak and longer exposure times were required. After dissolution of the callosic walls, JIM5 labeled the surface of microspores (Fig. 9, I–P; for stage **10/11**, see Fig. 9K). JIM5 labeling gradually decreased but was detectable until the end of stage **12M** (Fig. 9L). In contrast, JIM5 labeling was largely absent in the walls of developing *kns4* microspores (Fig. 9, M–P).

Developing tetrads and microspores were also isolated and immunolabeled using the JIM7 and JIM5 antibodies (Fig. 10). As in undissected anthers (Fig. 9, B and F), primary cell walls of both wild-type and *kns4* tetrads were labeled with JIM7 in a relatively uniform manner (compare Fig. 10, A and C). JIM7 labeling was also observed on the surface of Fig. 9, I–P microspores through stages **9L** to **12E**, with maximum intensity at stage **10/11** (Fig. 10B). In general, weaker labeling appeared on the surface of *kns4* microspores although some parts were as strongly labeled as wild type (Fig. 10D), suggesting HG deposition was unevenly distributed in the mutant.

The wild-type tetrad wall also showed a relatively even labeling pattern with JIM5 (Fig. 10E), although the labeling was never observed in resin-embedded sections (Fig. 9J). In contrast, primary walls of the *kns4* tetrads often displayed a partial labeling pattern (Fig. 10I), indicating that HG demethylesterification occurs only locally in the mutant. JIM5 also labeled the surface of wild-type microspores (Fig. 10, F–H). The labeling was initially observed at the end of stage **9M**, when the microspores were still within tetrads (Fig. 10E), reached a maximum at stage **10/11** (Fig. 10G), and then decreased thereafter (Fig. 10H). In contrast, the *kns4* microspores were labeled only weakly and partially with JIM5 (Fig. 10, J–L), similar to the labeling pattern observed with JIM7 (Fig. 10D).

Enlarged optical sections of JIM5-labeled wild-type stage **9L** microspores revealed that the less methylesterified HG is localized in exine cavities, between the nexine and tectum (Fig. 10M), but in later stages it forms a distinct layer at the base of exine cavities on nexine I (stage **12E**, Fig. 10O). Tangential optical sections near the surface showed that the JIM5-labeled HG at stage **9L** is located in the lacunae of the reticulate exine (Fig. 10N). This location is different from that of the AGPs, which cover the outer reticulate tectum surface at the same developmental stage (Fig. 7G). At stage **12E**, JIM5-labeled HG on nexine I is still distributed in a pattern that is opposite to the reticulate surface of the exine (Fig. 10P). Similar to wild type, the pectin deposited on *kns4* microspores filled the shallow cavities of the exine (Fig. 10, Q–T).

kns4 Pollen Defects Lead to Reduced Fertility

Given the AGP and pectin defects observed during microspore development in the *kns4* mutant, we wanted to determine the possible function(s) of *KNS4* in planta, especially during sexual reproduction. Because fruit length has previously been shown to be correlated with seed set (Barendse et al., 1986), fruits of wild type (Col-0) and *kns4* mutants were collected and their lengths measured. Fruits of *kns4* mutant plants were significantly shorter (*kns4-2*: 1.37 $\pm$ 0.03 cm; *kns4-3*: 1.35 $\pm$ 0.03 cm,

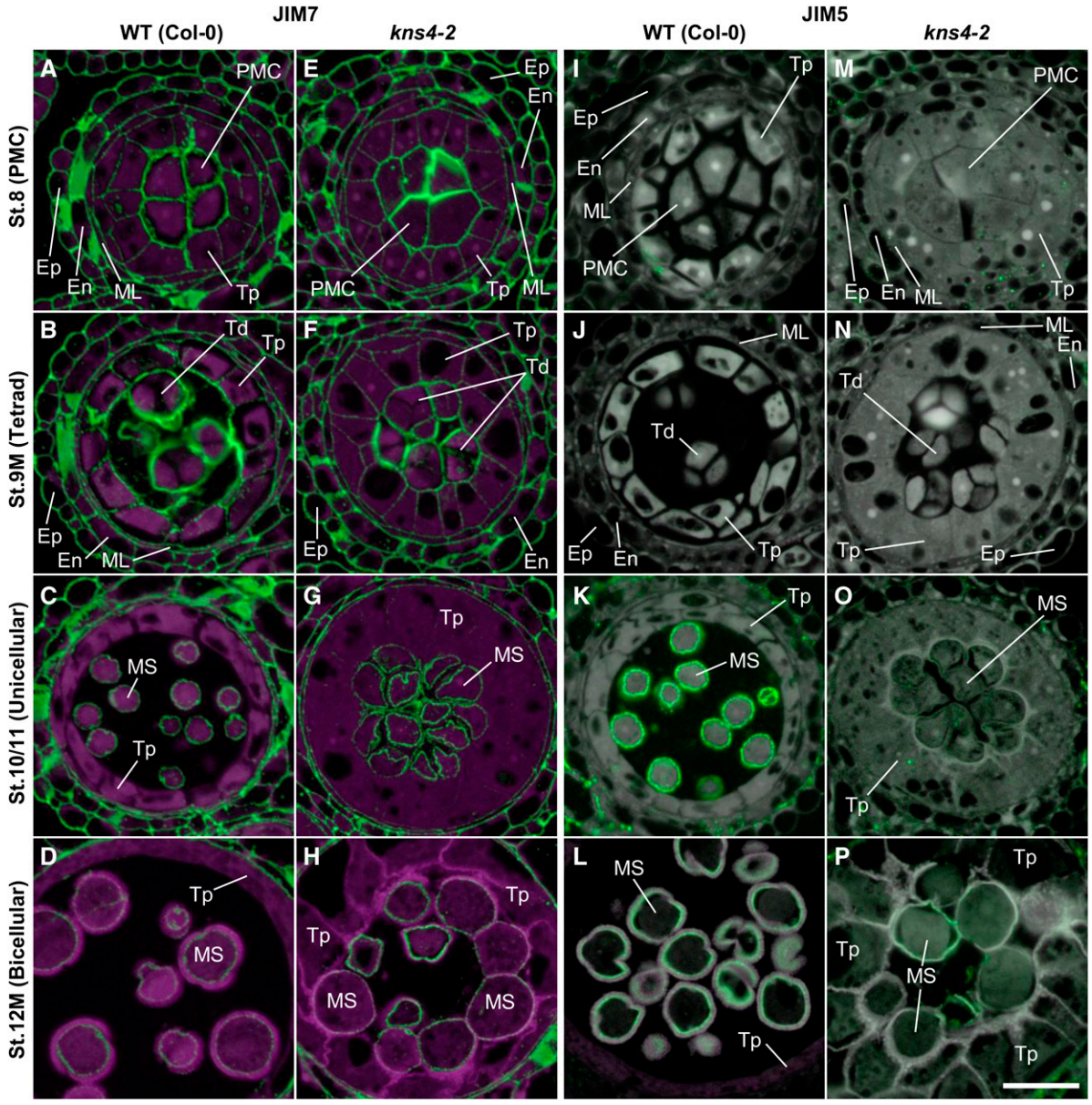

Figure 9. Fluorescence micrographs of the distribution of JIM7- and JIM5-epitope labeling of pectins within anthers. Cross sections of resin-embedded anthers of wild type (Col-0; A–D and I–L) and *kns4-2* (E–H and M–P) from stages **8** to **12M** were incubated with either JIM7 (A to H) or JIM5 antibody (I to P), and subsequently with Alexa Fluor 488-labeled secondary antibody. Fluorescence of Alexa Fluor 488 (green) and autofluorescence (magenta) were captured separately by epifluorescence microscopy and overlaid. Note that the exposure time for capturing JIM5 signals is longer than that for JIM7, resulting in relatively higher background in JIM5 images. En, Endothecium; Ep, epidermis; ML, middle layer cell; MS, microspore; PMC, pollen mother cell; Td, tetrad; Tp, tapetal cell. Bar = 20 μm.

n = 15) than those from wild type (1.67 ± 0.03 cm, n = 15, $P < 0.001$; Fig. 11A). Examination of the number of seeds present in each wild-type and *kns4* fruit at stage **17** (fully expanded green fruit, Smyth et al., 1990) showed that the loss of *KNS4* function reduced seed set by as much as 50% (wild type: 43 ± 1; *kns4-2*: 29 ± 2; *kns4-3*: 20 ± 2, n = 15, $P < 0.001$), although no bias toward the upper or lower half of the fruit was observed (Fig. 11, B and C).

To confirm that the reduced fertility observed in *kns4* mutants was a consequence of a disruption in male gametophyte development, reciprocal crosses were performed. When wild-type pollen was used to pollinate *kns4-2* pistils, fruits with normal lengths (1.51 ± 0.04 cm) resulted, whereas *kns4-2* pollen on wild-type pistils yielded significantly shorter fruits (0.86 ± 0.06 cm) with few fertilized ovules (Fig. 11D). These results suggested that *kns4* pollen grains have reduced

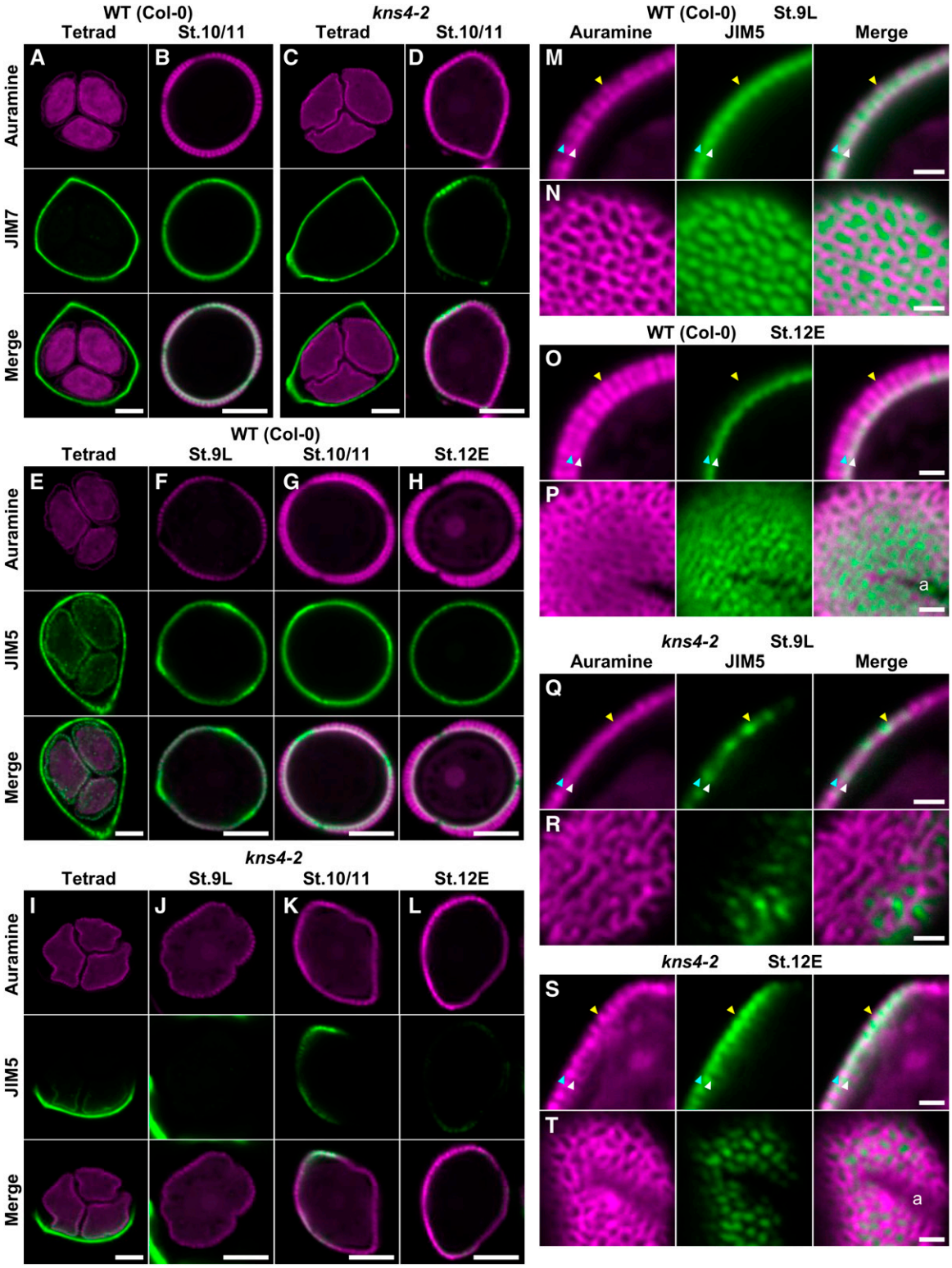

Figure 10. Fluorescence micrographs of the distribution of JIM7- and JIM5-epitope labeled pectins on the surface of isolated tetrads and developing microspores. A to D, Median optical sections of JIM7-labeled tetrads isolated from stage **9M** anthers (A and C) and microspores isolated from stage **10/11** anthers (B and D), respectively. Exine was visualized by auramine O staining. Specimens were observed by CLSM in which magenta and green channels show fluorescence of auramine O and Alexa Fluor 546, respectively. Wild type (A and B) and *kns4-2* (C and D) are compared. E to L, Median optical sections of JIM5-labeled tetrads (E and I) isolated from stage **9M** anthers and microspores (F–H and J–L isolated from anthers at indicated stages. Wild type (Col-0;

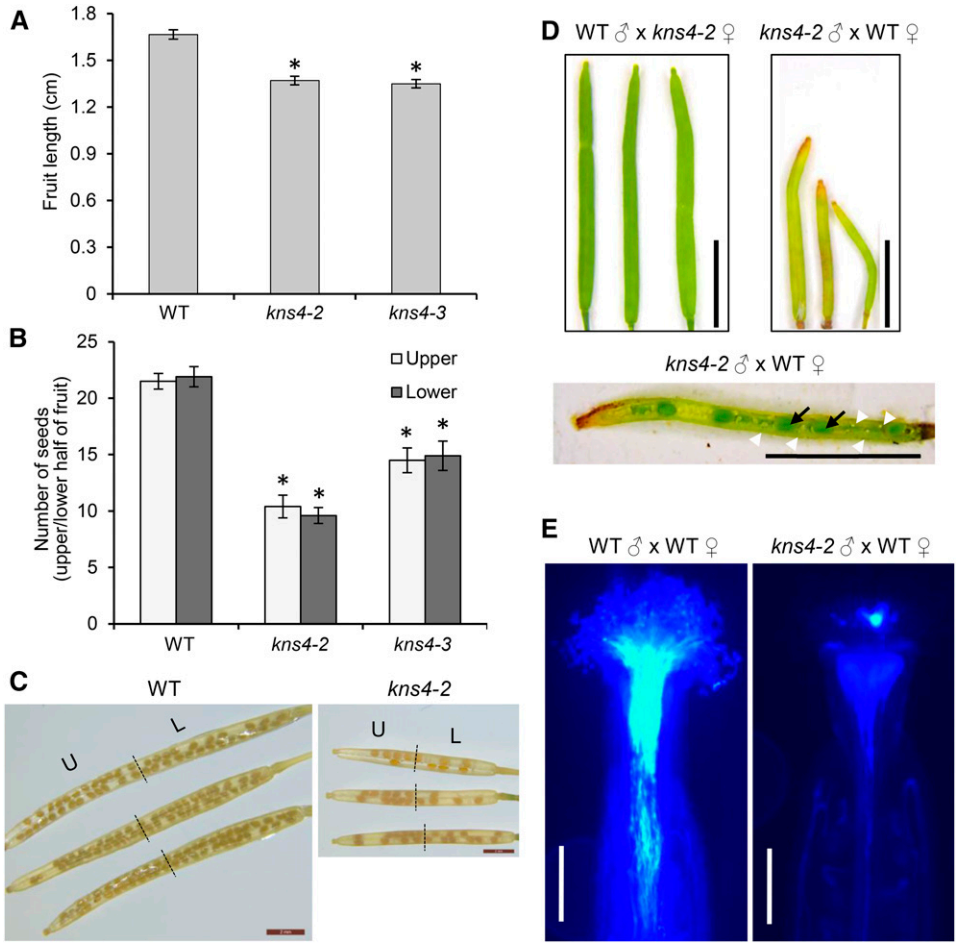

Figure 11. *kns4* has defects in sexual reproduction. A to C, Morphological phenotypes of fully elongated fruit length (A) and seed set (number of seeds per upper and lower half of fruit; B and C) were observed and quantified. Error bars indicate SD. *$P < 0.0001$ in a Student's *t*-test, wild type (Col-0) compared to *kns4-2* and *kns4-3* in (A) and (B). D, Reciprocal crosses between wild type and *kns4-2*. Fruits 7 d after pollination are shown. Dissection of fruits from *kns4-2*-pollinated wild-type pistils revealed formation of fewer seeds (black arrows) and many unfertilized ovules (white arrowheads), indicating lower probability of ovule fertilization by *kns4* pollen. E, wild-type, or *kns4-2* pollen tubes growing in vivo in manually pollinated wild-type pistils stained with aniline blue after 24 h. Staining appears as a bright light blue color. Scale bar = 2 mm in (C), 500 μm in (D) and 5 mm in (E). L, lower; U, upper.

fertility. Alexander staining to test for pollen viability showed most of the *kns4-2* pollen grains were colored purple, indicating they were viable (Fig. 12C). However, DAPI staining revealed that one-third of *kns4-2* pollen grains were developmentally aborted before entering tricellular stage (Fig. 12, B, D, and E). Hence, mutations in *KNS4* cause not only an exine abnormality but also a defect in pollen development.

Because pollen grains produced by stamens in a flower are in large excess of ovules in a pistil, developmental defects in a subset of pollen grains usually pose few, if any problems with self-pollination. However, observations of self-pollinated pistils revealed that the number of pollen grains that adhered to the stigma was far fewer in *kns4-2* than in wild type (Col-0; compare Fig. 12, G and F, respectively), indicating that the pollen clumps formed in *kns4* anthers affect pollen dispersal. Furthermore, it is also possible that *kns4* pollen grains are functionally less active. To examine this possibility, we tested if the pollen grains of *kns4* mutants could germinate, and that pollen tubes could extend down into the style. To do this we used an in vivo pollen tube growth assay, where pre-emasculated mature wild-type (Col-0) pistils were pollinated with either wild-type (Col-0) or *kns4-2* pollen grains, and pollen tube elongation observed after 24 h (Fig. 11E). Fewer *kns4* pollen tubes grew into the pistil compared to wild type, suggesting pollen tube germination and/or growth was compromised in the mutant. Deficiency in pollen tube elongation of *kns4-2* pollen grains were also observed in an in vitro pollen tube growth assay (Fig. 12H). Taken together, these data suggest that loss of *KNS4* function leads to multiple cell wall defects

Figure 10. (*Continued.*)
E–H) and *kns4-2* (I–L) are compared. M to T, Enlarged optical sections of JIM5-labeled microspores. Median optical sections showing exine longitudinal sections (M, O, Q, and S) and tangential optical sections that cut the surface of microspore (N, P, R, and T) or that cut baculae transversely (O). Microspores were isolated from stage **9L** (M, N, Q, and R) and stage **12E** (O, P, S, and T) anthers. Wild type (M–P) and *kns4-2* (Q–T) are compared. Blue, white, and yellow arrowheads indicate top and bottom boundary of the pectin layer, and the top of representative bacula, respectively. a, aperture. Bars = 5 μm in (A–L), and 1 μm in (M–T).

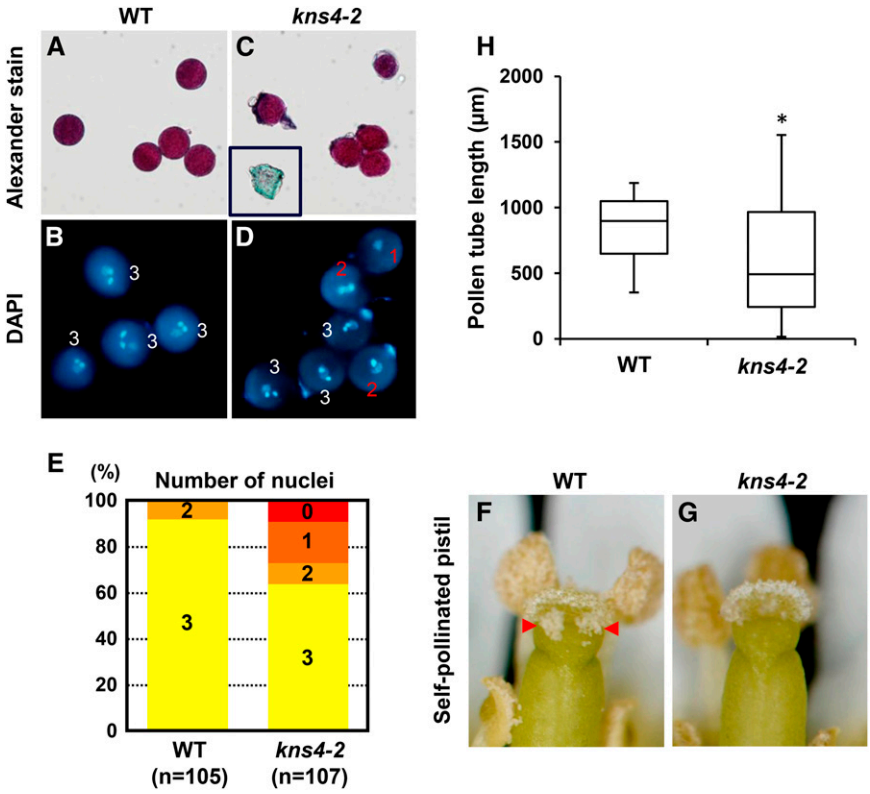

Figure 12. Viability of wild-type and *kns4-2* pollen grains. A to E, Staining of wild-type (Col-0) and *kns4-2* pollen grains with Alexander dye (A and C, respectively) and DAPI (B and D, respectively). A few aborted pollen grains are observed in the *kns4-2* pollen population (inset in C). The numbers in (B) and (D) show the number of nuclei in each pollen grain; (E) shows the percentage of wild-type and *kns4-2* pollen grains with 0, 1, 2, or 3 nuclei. F and G, Images of self-pollinated pistils in wild-type (Col-0; F) and *kns4-2* (G) flowers. Pollen adhesion is more obvious on the wild-type stigma (red arrowheads). H, Lengths of wild-type (Col-0) and *kns4-2* pollen tubes grown in vitro for 16 h as represented by a bar-and-whiskers plot ($n = 28$). $^*P < 0.01$ (Student's *t*-test).

during male gametogenesis that have developmental/reproductive consequences.

DISCUSSION

We have identified and characterized the gene defective in *kns4* mutants that results in a unique thin exine phenotype among 12 previously reported *kns* mutants (Suzuki et al., 2008). The *KNS4* gene is *At1g33430* and is identical to the underlying gene of the *upex1* mutant [Dobritsa et al., 2011; Li et al., 2017 (accompanying article)]. *KNS4* expression is restricted to tapetal cells in young anthers from stages **8** to **12E** of flower development, consistent with the timing of exine development (Smyth et al., 1990). Our biochemical studies demonstrate that KNS4 is a β-(1,3)-GalT involved in the biosynthesis of the β-(1,3)-galactan backbone of type II AGs. Type II AGs are found in both pectins as side chains of RG-I and AGPs; however, because changes in both AGPs and pectins were observed at the same stage of development in the tapetum of wild-type and *kns4* anthers, it is difficult to discern the exact molecular target of KNS4. That *kns4* mutants display a relatively severe phenotype also indicates that KNS4 is not redundant with other GalTs that are likely expressed in tapetal cells.

Exine formation is initiated with the construction of its basic structure composed of baculae and tectum in the primexine layer between the callosic wall and microspore plasma membrane in tetrads. We found that JIM8-labeled AGPs are a constituent of primexine in tetrads (Fig. 6B), together with previously identified pectin (HG and RG-II; Rhee and Somerville, 1998). Furthermore, JIM8- and MAC204-labeled AGPs, as well as JIM5- and JIM7-labeled HGs, form matrix layers on the surface of free microspores after being released from tetrads (Figs. 6–10). Although the basic structure of the exine has been established in tetrads, its thickness increases more than 2-fold by stage **12E** (Supplemental Fig. S1A). Therefore, it is expected that the matrix of AGP and pectin functions as a framework for sporopollenin deposition on the surface of free microspores at stages **9L** to **12E**. Because it is proposed that sporopollenin is transferred from tapetal cells to the microspore surface as either copolymers or fine fibrillar materials (Owen and Makaroff 1995; Quilichini et al., 2010), AGPs (and pectins, and possibility other, as yet unidentified, polysaccharides/glycoproteins) may also be incorporated in the copolymers and transferred concomitantly with sporopollenin. We propose a model of how AGPs and pectins might function in the construction of exine (Fig. 13). By stage **9L**, a framework of exine is made in the primexine layer that is mainly composed of pectin. AGPs are laid down over the pectin but initially, they do not enter into the exine cavities. The AGP layer is reticulate and displays a similar pattern to exine. During microspore development, sporopollenin supplied by tapetal cells is deposited onto the expanding exine. AGPs are also

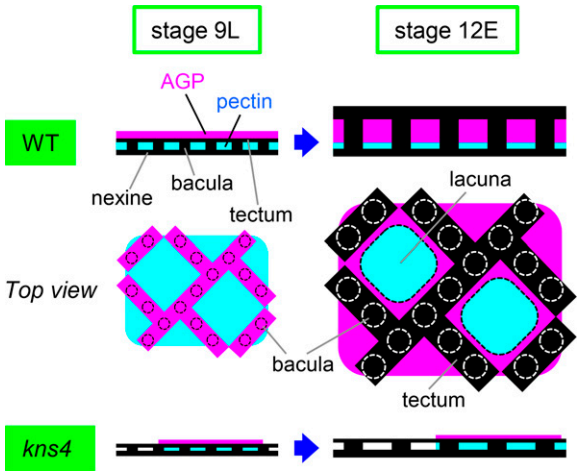

Figure 13. Schematic model of the function of microspore primexine in exine development. On the surface of wild-type microspores just released from the tetrad (stage **9L**), the tectum of developing exine is sandwiched between pectin and AGP. The top view indicates AGPs lie on the outer surface of the tectum and display a similar reticulate pattern, and pectins show an internal distribution. As microspores develop, AGPs and sporopollenin supplied by tapetal cells are deposited into the primexine and exine, respectively. By stage **12E**, the AGP layer laid down over the pectins becomes thicker, lifts the tectum up, and extends the baculae, resulting in exine thickening. AGPs fill the exine cavities except for baculae and lacunae, whereas pectins remain in the lacunae. In *kns4*, the AGP and pectin layers are incompletely formed at stage **9L**. Subsequent deposition of AGP and sporopollenin is reduced and the exine remains thin at stage **12E**.

supplied by tapetal cells and are deposited into the AGP layer, the thickening of which elongates the baculae and raises the tectum. At stage **12E**, a thin pectin layer remains at the bottom of the exine cavities and the thickened AGP layer fills the space beneath the tectum. According to this model, the thin exine phenotype of the *kns4* mutants is well explained by the observed defects in pectins and/or AGPs. The uneven thickness of exine observed in the mutant is likely due to the uneven distribution of AGP and pectins and is consistent with the nonuniform labeling of AGP and pectin epitopes seen in Figures 7 and 10. It is also conceivable that other matrix phase polysaccharides act as the framework that regulate the size of the lacunae and impact on the 3D architecture of the pollen wall.

The interactions (covalent and/or noncovalent) between pectins and AGPs has been reported in numerous studies (Baldwin et al., 1993; Li et al., 1995; Jauh and Lord, 1996; Mollet et al., 2002; Majewska-Sawka and Rodriguez-Garcia, 2006) and structural analyses have provided multiple lines of evidence that AGPs are associated with pectins, especially RG-I (Immerzeel et al., 2006; Mohnen, 2008; Caffall and Mohnen, 2009) and more recently xylan (Tan et al., 2013; Voiniciuc et al., 2015). Moreover, SOS5/FLA4 (At3g46550), a fasciclin-like GPI-anchored AGP, was recently shown to be involved in the formation of either a pectin or a pectin-hemicellulose network in seed mucilage (Griffiths et al., 2014). Although the distribution of AGPs and pectins are not identical in primexine, AGPs and/or pectins and possibly xylan (Li et al., 2017) might function as a scaffold for other wall components and could potentially be cross-linked to each other.

The first developmental abnormality identified in *kns4* anthers was the failure of PMC separation before meiosis (stage **9E**), a defect that continues into stage **9M** when PMCs become tetrads (Fig. 2). It has been proposed that pectin plays an important role in both cell adhesion and cell separation in plant organ development (Micheli, 2001; Pelloux et al., 2007; Wolf and Greiner, 2012). We detected differences between wild type and *kns4* both in the deposition of AGPs (Figs. 6, E and F and 7D) and in the demethylesterification of HG (Fig. 10I) in the walls of tetrads, although changes to AGP epitope labeling were initially observed in PMC walls (stage **8**). Therefore, the apparent reduction in abundance of AGPs slightly precedes the changes observed in pectin, suggesting AGPs are the more likely direct target of KNS4 activity. While highly methylesterified HG pectin appeared to be deposited in a normal manner in *kns4* mutant microspores (Figs. 9, E and F and 10C), the appearance of less-methylesterified HG pectin as revealed by JIM5 labeling was patchy (Fig. 10I) unlike wild type where the labeling is relatively uniform (Fig. 10E). This suggests there is an accessibility issue of these walls to the pectin methylesterases that demethylesterify pectin. After degradation of the tetrad wall, released microspores of the *kns4* mutants still adhered to each other (Fig. 2, J–L) and no additional JIM5 epitopes were revealed (Fig. 10, J–L) when normally signal would increase (Fig. 10G; stage **10/11**). Hence, reduced accessibility to *kns4* microspore walls persists after tetrad wall dissolution. We showed that mutant microspores at stage **12E** formed a clump when they were extruded from anthers and that callosic walls abnormally remained between microspores (Fig. 3H). Furthermore, Li et al. (2017) have shown the existence of abnormally remaining xylan around microspores. From these results, it seems likely that the AGPs and/or pectins produced by the enzymatic function of KNS4 contribute to cell wall architecture in a way that impacts the accessibility of glycan hydrolytic enzymes (glycosyl hydrolases) to the locular space.

The second abnormality relates to the deposition of the sporopollenin. Sporopollenin is synthesized in tapetal cells, secreted to locules, and transferred to the microspore surface (Owen and Makaroff 1995; Quilichini et al., 2014). Besides the failure of exine formation in *kns4*, we revealed that the sporopollenin is abnormally deposited on the surface of tapetal cell walls, which is in contact with the developing exine of microspores (Figs. 2, R–T and 3, D–F). In wild type, tapetal walls are usually degraded and have disappeared by stage **12L** when tapetal cells collapse. In contrast, *kns4* mutant walls fail to degrade completely, remaining attached to the surface of microspores (Figs. 2L and 3F).

The third abnormality of *kns4* mutants is related to microspore development and pollen fertility, issues that are likely consequences of abnormal pollen development. We studied the reproductive success of *kns4*

pollen with reciprocal crosses between wild type and the *kns4-2* mutant showing reduced seed set in *kns4* (Fig. 11D). Likewise, for self-pollinated mutants, the fruits were shorter compared to wild type (Fig. 11, A–C). In addition, an in vivo pollen tube growth assay indicated that fewer pollen tubes germinated and grew into the style (Fig. 11E). DAPI staining revealed that one-third of *kns4* microspores abort before generative cell mitosis (Fig. 12, B–E). As a consequence, the mutants show reduced seed set (Fig. 11). These results suggest that the microspore phenotype has an impact on the reproductive success of *kns4*. Considerable evidence has now accumulated implicating the involvement of AGPs in pollen fertility and pollen tube growth (for review, see Nguema-Ona et al., 2012, Pereira et al., 2015). KNS4, as a β-(1,3)-GalT, is predicted to be involved in the synthesis of β-(1,3)-galactan backbone of type II AGs, which can either be attached to AGPs or pectin. It is possible that KNS4 has multiple cell wall polysaccharide targets in pollen; hence, knocking out *KNS4* leads to a severe microspore phenotype, which results in reduced pollen fertility.

KNS4/UPEX1 encodes a β-(1,3)-GalT responsible for type II AG biosynthesis on either the protein backbones AGPs or the side chains of the pectic polysaccharide RG-I. This study, together with that of the accompanying article by Li et al., (2017), demonstrates that the absence of these glycans leads to severe defects in primexine and exine formation and subsequent microspore development.

MATERIALS AND METHODS

Source and Growth of Plants

The *kns4-1* mutant allele in the Landsberg *erecta* background of Arabidopsis (*Arabidopsis thaliana*) was previously described in Suzuki et al. (2008). T-DNA insertion alleles in the Columbia-0 (Col-0) background, SALK_091466 (*kns4-2*) and SAIL_544_C02 (*kns4-3*), were obtained from the Arabidopsis Biological Resource Centre (Ohio State University). Arabidopsis seeds were sown directly on soil, stratified at 4°C for 3 d, and grown under a regime of 16 h light at 21°C and 8 h darkness at 17°C. *Nicotiana benthamiana* plants were grown in soil (Debco seed raising mix, Tyabb) at 20° to 26°C in a glasshouse under continuous cool-white lights supplemented with daylight for 5 to 6 weeks.

Electron Microscopy and Immunolabeling

For SEM observations of pollen grains and TEM observations of anther sections, the methods as described by Suzuki et al. (2008) were followed. Immunogold labeling was carried out as described in Wilson and Bacic (2012).

Immunofluorescence Labeling

Flower bud clusters at inflorescence apices were fixed [2% (v/v) formaldehyde, 2.5% (v/v) glutaraldehyde, 25 mM Na-P buffer, pH 7.5] for 24 h at 4°C, then dehydrated through an ethanol series. The ethanol was replaced with 1:1 mix of LR White resin (type medium; Electron Microscopy Sciences) and ethanol, then with pure resin. The resin-infiltrated samples were placed separately in small plastic tubes, and polymerized by heat treatment at 50°C for 12 h in a plastic bag containing oxygen absorber. Sections (1–2 μm) were cut in a microtome (RM2125RT; Leica) equipped with TC-65 blade and mounted on a slide (MAS-coated glass slide; Matsunami). Sections were treated with a solution (1% (w/v) bovine serum albumin (BSA) in PBST (5.1 mM Na_2HPO_4, 1.6 mM KH_2PO_4, 130 mM NaCl, 0.02% Tween 20) for 1 h at RT for blocking, and subsequently incubated with a 1:40 dilution of primary antibody in the same solution for 4 h at RT with gentle rocking. Rat monoclonal antibodies JIM5, JIM7, JIM8, and MAC204 (CarboSource Service) were used as primary antibodies. After washing with PBST, samples were reacted with a 1:100 dilution of secondary antibody (Alexa Fluor 488 Goat anti-Rat IgG; Thermo Fisher Scientific) for 2 h and then washed with PBST and mounted with aqua-poly/mount (Polysciences). A BX60 epifluorescence microscope equipped with a DP72 digital camera (Olympus) was used for observation. Fluorescence of Alexa Fluor 488 and background autofluorescence of the sample were captured under fluorescence mirror units NIBA and WBV, respectively. To make a merged image of these signals, the NIBA and WBV images were captured simultaneously, split into RGB channels by Photoshop (Adobe), and both the R and B channels of the NIBA image were replaced with the G channel of the WBV image.

Anthers collected from developing flower buds were immersed into fixative (3.7% formaldehyde, 50 mM Na P buffer, pH7.2), ground with a homogenizer (BioMasher II; Nippi) and put on ice for 1 h. After tissue debris were removed, tetrads and microspores were collected by centrifugation at 400*g* for 1 min, washed three times with PBST, treated with a blocking solution (1% (w/v) BSA in PBST), and incubated with a 1:100 dilution of primary antibody in blocking solution for 3 h at RT. Samples were washed twice with PBST, rinsed with blocking solution, and then incubated with a 1:100 dilution of secondary antibody (Alexa Fluor 546 Goat anti-Rat IgG, Thermo Fisher Scientific) for 1 h. After washing twice with PBST, samples were suspended in 0.5 × PBS (2.6 mM Na_2HPO_4, 0.8 mM KH_2PO_4, 65 mM NaCl), 0.005% (w/v) Tween 20, 18% (v/v) glycerol, 0.005% (w/v) auramine O. The sample was spread on a coverslip coated with 0.2% (v/v) polyethyleneimine solution and mounted on a glass slide. The specimens were observed by a CLSM (FV1000; Olympus) with Ex: 473 nm, Em: 485 to 545 nm for auramine O staining, and Ex: 559 nm, Em: 565 to 665 nm for Alexa Fluor 546.

Yariv Dye Staining of Arabidopsis Pollen

Floral buds at stage **12** (Smyth et al., 1990) were collected from five plants of each genotype (wild type, *kns4-2*, and *kns4-3*) and anthers dissected with a fine blade. The dissected anthers were then placed into either α-Gal Yariv reagent dye [40 μL of 2 mg/mL in 1% (w/v) NaCl] as a negative control or β-Glc Yariv reagent dye [40 μL of 2 mg/mL in 1% (w/v) NaCl] to stain for AGPs. The samples were tapped gently to release the pollen and then placed in a ThermoMixer (Eppendorf) at 800 rpm for 20 min, both to assist pollen release and dye infiltration. The samples were incubated at 4°C overnight and subsequently washed twice with 0.15 M NaCl before viewing under a light microscope.

Toluidine Blue Staining

Sections (1 μm) of resin-embedded anthers as prepared for TEM were mounted on a glass slide, stained with a toluidine blue staining solution [0.5% (w/v) toluidine blue, 0.5% (w/v) sodium borate], and the slides heated on a hot plate for 20 min. After washing out the stain, the specimen was viewed under a light microscope (BX60; Olympus).

Calcofluor Staining

Sections (8 μm) of paraffin-embedded flower bud clusters were mounted on a MAS-coated glass slide, deparaffinized by a serial treatment with Lemosole (Wako Pure Chemical), 1:1 mix of Lemosole and ethanol, then ethanol, and rehydrated by an ethanol series. The sample was incubated with 1% (w/v) Calcofluor White (Fluorescent Brightener 28; Sigma-Aldrich) for 5 min, washed five times with water, and sealed with aqua-poly/mount. Fluorescence was detected by an epifluorescence microscope (BX60; Olympus) with a WBV mirror unit.

Aniline Blue Staining of Anther Sections

Sections of resin-embedded anthers were incubated with aniline blue fluorochrome (0.1 mg/mL; Biosupplies) and sealed with aqua-poly/mount. The specimens were observed by a CLSM (FV1000; Olympus) with Ex 405 nm, Em 485-555 nm for aniline blue staining, and Ex 440 nm, Em 610–710 nm for autofluorescence of sporopollenin.

Measurement of Exine Thickness

Median optical sections of developing microspores prepared for immunofluorescence labeling were used to measure exine thickness by CLSM. Local maxima of exine thickness were measured at three positions in a microspore, and

average and SD of 30 measurements (10 microspores for each developmental stage) was calculated. Intine and exine thickness were also measured using labeled and unlabeled TEM sections.

Evaluation of Seed Set Activity

The fruits from self-pollinated *kns4-2*, *kns4-3* and wild type (Col-0) were collected and the individual fruit length measured. Fruits were decolorized with 90% acetone for 30 min, followed by 50% ethanol for 30 min, and 70% ethanol overnight to view contents. After a further 70% ethanol wash for 30 min, samples were incubated for an additional 30 min in 100% ethanol. Fruits were then viewed under a model no. M205A stereo microscope (Leica Microsystems), and seeds counted.

Reciprocal crosses were performed between wild type and *kns4-2* following the protocol from Weigel and Glazebrook (2002). Ten flowers from each line were emasculated and hand-pollinated with the appropriate pollen type. Fruits were allowed to develop for a week before images were captured using a model no. M205A stereo microscope (Leica Microsystems). Two biological replicates comprising 10 flowers for each line were performed for the reciprocal crosses. The fruits were then dissected and the embryos and ovules were checked for any developmental defects.

Pollen Tube Growth

The in vivo pollen tube growth protocol of Wu et al. (2010) was followed. Imaging was carried out using a model no. DM 6000B compound light microscope utilizing a 5× objective (Leica Microsystems) under an I3 filter (BP 450-490; Excitation: LP 515 nm).

Mapping of the *kns4-1* Mutation

A F2 population obtained by a cross between *kns4-1* and Col-0 was used for a mapping the *KNS4* locus using the method described by Suzuki et al. (2008).

Genetic Complementation

The *KNS4* promoter region (*ProKNS4*, 2006 bp upstream of the initiation codon) was amplified by PCR from Col-0 genomic DNA using KNS4p-attB4-F (5′-GGGGACAACTTTGTATAGAAAAGTTGTATCATCTTCAACACCATCTTAGCT-3′) and KNS4p-attB1-R (5′-GGGGACTGCTTTTTTGTACAAACTTGTGAAAACAAGAATGTAGTTGCAGAA-3′) primers. The amplified fragment was cloned into pDONR P4-P1R vector by a Gateway BP reaction (Invitrogen) to make a promoter entry clone, pDONR-L4KNS4pR1. The coding region of *KNS4* was PCR-amplified from Col-0 inflorescence first-strand cDNA using KNS4-attB1-F (5′-GGGGACAAGTTTGTACAAAAAAGCAGGCTTTTTATATAAATAACATCTCCTCAACATTC-3′) and KNS4-attB2-R (5′-GGGGACCACTTTGTACAAGAAAGCTGGGTAGACGAAGAAGCGAAAATTAGCTAGA-3′) primers, and cloned into the pDONR201 vector by a BP reaction to make a CDS entry clone, pDONR-KNS4. PrimeSTAR HS DNA polymerase (Takara Bio) was used for cloning PCRs. The promoter and CDS were joined and transferred to a binary vector, R4pGWB401 (Nakagawa et al., 2008) by a Gateway LR reaction (Invitrogen) to generate the binary plasmid pGWB-KNS4p:KNS4. This plasmid was introduced into *Agrobacterium tumefaciens* strain C58C1 (pMP90) by electroporation and the bacteria then used to infect *kns4-1* plants by floral dip (Ishiguro et al., 2010). Transformants were identified on agar plates supplemented with 30 mg/L kanamycin.

RT-PCR

RNA was extracted from various organs using the RNeasy Mini Kit (Qiagen) and incubated with DNase I to remove residual DNA. First strand cDNA was synthesized using SuperScript III reverse transcriptase (Invitrogen) primed with an oligo$(dT)_{20}$ primer. PCRs were carried out to amplify a part of coding region using Ex Taq DNA polymerase (Takara Bio). *ACT2* (*At3g18780*) was used as a control. Primers used for PCR were as follows: KNS4-F2 (5′-GAGAACTCACCAAGCAGTTA-3′), KNS4-R2 (5′-CCTGTTGCATGCCTAAAGTA-3′), ACT2-F (5′-GAAGAGCACCCTGTTCTTCT-3′), and ACT2-R (5′-TTCTCGATGGAAGAGCTGGT-3′).

To determine mRNA levels in developing anthers, ReverTra Ace qPCR RT Master Mix with gDNA Remover (Toyobo) was used for preparing first strand cDNA. Real-time qRT-PCR was performed using the SYBR Premix Ex Taq II (Takara) on a LightCycler 480 (Roche). *PDF2* (*At1g13320*) was used as an internal control. Primers used for qRT-PCR were as follows: *KNS4*, 5′-GAGAACTCACCAAGCAGTAA-3′ and TTTCTGCAGACGGCTCTGGTTTTTC-3′; *PDF2*, 5′-TAACGTGGCCAAAATGATGC-3′ and 5′-GTTCTCCACAACCGCTTGGT-3′.

In Situ Hybridization

A DNA fragment corresponding to a half of a *KNS4* mRNA sequence was prepared by PCR amplification with two primers KNS4-*Sac*I-F (5′-CCCGAGCTCTTTTATATAAATAACATCTCCTCAACATTC-3′) and KNS4-*Sac*I-R2 (5′-CCCGAGCTCAGAAGTACAGTCTTGTCTTTGTCGA-3′) and cloned in both directions into the *Sac*I site of the pBS-KS(+) plasmid. The resulting two plasmids, pBS-KNS4ΔC3f and pBS-KNS4ΔC3r, contain the sense and antisense orientation of the *KNS4* sequence, respectively, relative to the direction of T7 promoter. A DNA fragment was amplified from each plasmid by PCR using M460 and RV58 primers, and purified using the QIAquick PCR purification kit (Qiagen). The purified fragment derived from pBS-KNS4ΔC3f was transcribed in vitro by T7 RNA polymerase in the presence of Fluorescein labeling mix (Roche, Switzerland) to prepare a fluorescein-labeled sense probe for *KNS4*. An antisense probe was prepared from a fragment derived from pBS-KNS4ΔC3r in a similar manner. To remove unincorporated nucleotides, transcripts were purified by a ProbeQuant G-50 Micro Column (GE Healthcare).

Flower bud clusters were fixed in a fixative [3.7% (v/v) formaldehyde, 5% (v/v) acetic acid, 50% (v/v) ethanol] for 15 h at RT. Samples were dehydrated in a graded ethanol series, immersed in Lemosole, and embedded in paraffin (Paraplast Plus; McCormic Scientific). Serial sections of 8 μm thick were prepared by a microtome, mounted on a MAS-coated glass slide, deparaffinized by Lemosole, and rehydrated with a graded ethanol series. Samples were treated with 5 μg/mL proteinase K for 30 min at 37°C in a buffer (100 mM Tris-HCl, 50 mM EDTA, pH7.5), fixed in freshly hydrolyzed 5% (v/v) paraformaldehyde in 10 mM Na-P buffer (pH 7.2), and acetylated in 0.5% (v/v) acetic anhydride dissolved in 100 mM triethylamine-HCl buffer (pH 8.0). Samples were washed in 2× SSPE and dehydrated in a graded ethanol series. Two-hundred microliters of hybridization mix [50% (v/v) formamide, 10 mM Tris-HCl, 0.3M NaCl, 1 mM EDTA, 1× Denhardt's solution, 10% dextran sulfate, 30 mM DTT, 1 μg/μL *Escherichia coli* tRNA, 1 μg/μL poly A, and 0.5 ng/μL sense or antisense probe] was placed on a slide and the slide incubated overnight at 50°C in a humid box. Samples were washed in 4× SSC at 50°C for 15 min, treated with 20 μg/mL RNase A in a buffer (10 mM Tris-HCl, 500 mM NaCl, 10 mM EDTA, pH 7.5), and washed twice in 0.5× SSC at 50°C for 20 min. The samples were then rinsed in buffer 1 (100 mM Tris-HCl, 150 mM NaCl, pH 7.5), treated with blocking solution (1% Blocking reagent (Roche) in buffer 1), and reacted with Anti-Fluorescein-AP (Roche) in buffer 2 (100 mM Tris-HCl, 150 mM NaCl, 0.2% (v/v) Tween 20, 1% (w/v) BSA, pH 7.5) for 2 h at RT. After washing in buffer 1, the slide was incubated in a stain solution (0.55 mM NBT, 0.43 mM BCIP, 100 mM Tris-HCl, 100 mM NaCl, 50 mM $MgCl_2$, pH 9.5) for 9 h at RT. After washing in TE (10 mM Tris-HCl, 1 mM EDTA, pH 7.5), samples were sealed with aqua-poly/mount.

Construction of *KNS4* Promoter-reporter Constructs

The same *KNS4* promoter fragment was PCR-amplified as described above and cloned into the pDONR201 vector by a Gateway BP reaction. The resulting plasmid, pDONR-L1KNS4pL2, was recombined with pGWB433 and pGWB450 (Nakagawa et al., 2007) by a Gateway LR reaction to produce pGWB-KNS4p:GUS (binary plasmid for GUS fusion) and pGWB-KNS4p:GFP (for GFP fusion), respectively. Plant transformations were carried out as described above.

Transient Expression of *KNS4* in *N. benthamiana* Leaves

Transient expression in *N. benthamiana* leaves was carried out following Lampugnani et al. (2016) with minor modifications. To generate the Pro-35S:*KNS4* construct, the *KNS4* CDS was amplified from cDNA of wild-type Arabidopsis floral buds using primers KNS4-Fwd (5′-TCGAGGAATTCGGTACCATGAGGGCGAAAGCTGCTTCGGG-3′) and KNS4-Rev (5′-AAGCAGGACTCTAGAGGATCCTCAGACGAAGAAGCGAAAATTAGC-3′). The PCR product was cloned into the binary vector pFUERTE (Wilson et al., 2015) by GeneArt seamless cloning according to the manufacturer's instructions (Invitrogen). Sequence-verified constructs along with the helper plasmid pSOUP were introduced into *A. tumefaciens* strain AGL1 via electroporation as described in Lampugnani et al. (2012). A 35S:VENUS construct was used as a transformation control (Wilson et al., 2015).

Microsomal Membrane Preparation from *N. benthamiana* Leaves

Microsomal membranes (MMs) were prepared according to Song et al. (2015) with minor modifications. Briefly, 2 g of plant tissue was ground using a mortar and pestle in 10 mL of chilled extraction buffer (0.1 M HEPES/KOH pH 6.8, 0.4 M Suc, 5 mM $MgCl_2$, 5 mM $MnCl_2$, 1 mM PMSF; Roche EDTA-free complete protease inhibitor). MM preparations were resuspended in 250 μL extraction buffer and stored at −80°C before use.

Biochemical Assay of KNS4

MMs were pretreated on ice for 10 min with 1% v/v Triton X-100 (Sigma-Aldrich) before use in a GalT biochemical activity assay. The GalT enzyme assay was conducted in a reaction volume of 50 μL consisting of detergent-permeabilized MM (100 μg total protein as determined by the Pierce BCA protein assay, using BSA as standard), 5 μM fluorescent acceptor [β-Gal-NBD; NBD = 7-nitro-2,1,3-benzoxadiazole; McGill and Williams (2009)] kindly provided by Professor Spencer Williams (Department of Chemistry, Bio21 Institute, The University of Melbourne), and 0.4 mM UDP-sugar (Sigma-Aldrich) as donor. The reaction mixture was incubated for 1 h at 25°C and subsequently terminated by adding 1 μL glacial acetic acid and 1 μL 0.5 M EGTA. The reaction mixture was then centrifuged for 2 min at maximum speed in a bench microfuge and the supernatant filtered using a 0.22 μm filter unit (Millipore). The filtrate was transferred to an HPLC vial for Reversed Phase-HPLC (RP-HPLC) analysis.

RP-HPLC Analysis of Biochemical Assay Products

Five microliters of enzyme assay product filtrate was analyzed by RP-HPLC using a Zorbax Eclipse XDB-C18 RP column (4.6 × 150 mm, 5 μm; Agilent Technologies) with the following step gradient profile: 0 to 1.0 min 25% B; 1.1 to 12.1 min 30% B; 12.2 to 17.2 min 80% B; 17.3 to 25.0 min 100% B where A: 50 mM ammonium acetate, pH 4.3 and B: acetonitrile, and the flow rate was 0.5 mL/min. NBD-tagged enzyme assay products were detected by a model no. FP-920 Intelligent Fluorescence Detector (Ex 470 nm, Em 540 nm; JASCO).

Enzymatic Characterization of Biochemical Assay Products

The enzyme assay product (10 μL; see above) was mixed with 17.5 μL 50 mM sodium acetate, pH 3.8 and digested with 2.5 μL of recombinant SGalase1, an exo-β-(1,3)-galactanase from *Streptomyces* sp. prepared according to the method of Ling et al., (2012). In parallel, 10 μL of GalT enzyme assay product was mixed with 17.5 μL extraction buffer (see above) and digested with 1.5 U (approximately 2.5 μL) of *E. coli* β-galactosidase (Grade VIII, *G5635*; Sigma-Aldrich). Both reactions were incubated at 37°C for 1 h and then terminated by heating at 95°C for 10 min, spun down, and the sample reanalyzed by RP-HPLC as described above.

Mass Spectrometric Characterization of Biochemical Assay Products

For mass spectrometry analysis of the enzyme assay reaction products, the entire filtered assay mixture was injected into the RP-HPLC column. Peaks were manually collected and analyzed by direct infusion ESI-MS on a QSTAR Elite hybrid quadrupole time-of-flight mass spectrometer (Sciex). The MS was operated in positive ion mode with an ion source voltage of 2200 V using 10 μm uncoated SilicaTips (New Objective). Analyst QS 2.0 software (Sciex) was used to collect data in data-dependent acquisition mode for the three most intense ions fulfilling the following criteria: m/z between 450 and 2000; ion intensity 40 counts; and charge state between +1 and +2. After MS/MS analysis, these ions were dynamically excluded for 18 s, using a mass tolerance of 50 mDa. MS scans were accumulated for 0.5 s, and MS/MS scans collected in automatic accumulation mode for a maximum of 2 s Mass and charge state-dependent rolling collision energy was used and the MS instrument was calibrated daily with [Glu]-fibrinopeptide B (Sigma-Aldrich).

To obtain a full scan of all the possible m/z peaks for the enzyme products, a nano LC-MS was performed. The sample was loaded onto a 300 μm × 5 mm Zorbax 300SB-C18 (Agilent Technologies) RP precolumn attached to a Prominence nano-LC system (Shimadzu). The precolumn was washed with 0.1% (v/v) formic acid in 5% (v/v) acetonitrile for 15 min before being placed in-line with a 75 μm i.d. × 150 mm Zorbax 300SB-C18 RP column (Agilent Technologies). Products were eluted using a gradient of 5% to 80% (v/v) acetonitrile in 0.1% (v/v) formic acid over 1 h, at a flow rate of 0.2 μL/min. Products with a charge state of either +1 or +2, between 300 D and 1500 D were analyzed via ESI-MS on a QSTAR Elite hybrid quadrupole time-of-flight mass spectrometer (Applied Biosystems/MDS Sciex) operated in the positive ion mode, as described above.

Supplemental Data

The following supplemental materials are available.

Supplemental Figure S1. The average exine thickness measured from CLSM and TEM images.

Supplemental Figure S2. Enzyme activity of KNS4 using different UDP-sugar donors.

Supplemental Figure S3. Transmission electron micrographs of stage **12M** wild-type and *kns4-2* microspores labeled with either anti-AGP (JIM8, JIM13) or anti-callose gold-labeled antibodies.

ACKNOWLEDGMENTS

We thank Professors Hitoshi Sakakibara and Kenzo Nakamura for helpful discussions and Rie Ishiguro and Fumika Ezuka for excellent technical assistance.

Received September 1, 2016; accepted November 6, 2016; published November 9, 2016.

LITERATURE CITED

Aarts MGM, Hodge R, Kalantidis K, Florack D, Wilson ZA, Mulligan BJ, Stiekema WJ, Scott R, Pereira A (1997) The *Arabidopsis MALE STERILITY 2* protein shares similarity with reductases in elongation/condensation complexes. Plant J **12:** 615–623

Aouali N, Laporte P, Clément C (2001) Pectin secretion and distribution in the anther during pollen development in *Lilium*. Planta **213:** 71–79

Ariizumi T, Hatakeyama K, Hinata K, Inatsugi R, Nishida I, Sato S, Kato T, Tabata S, Toriyama K (2004) Disruption of the novel plant protein NEF1 affects lipid accumulation in the plastids of the tapetum and exine formation of pollen, resulting in male sterility in *Arabidopsis thaliana*. Plant J **39:** 170–181

Ariizumi T, Hatakeyama K, Hinata K, Sato S, Kato T, Tabata S, Toriyama K (2003) A novel male-sterile mutant of *Arabidopsis thaliana*, *faceless pollen-1*, produces pollen with a smooth surface and an acetolysis-sensitive exine. Plant Mol Biol **53:** 107–116

Ariizumi T, Kawanabe T, Hatakeyama K, Sato S, Kato T, Tabata S, Toriyama K (2008) Ultrastructural characterization of exine development of the *transient defective exine 1* mutant suggests the existence of a factor involved in constructing reticulate exine architecture from sporopollenin aggregates. Plant Cell Physiol **49:** 58–67

Ariizumi T, Toriyama K (2011) Genetic regulation of sporopollenin synthesis and pollen exine development. Annu Rev Plant Biol **62:** 437–460

Baldwin TC, McCann MC, Roberts K (1993) A novel hydroxyproline-deficient arabinogalactan protein secreted by suspension-cultured cells of *Daucus carota* (purification and partial characterization). Plant Physiol **103:** 115–123

Barendse GWM, Kepczynski J, Karssen CM, Koornneef M (1986) The role of endogenous gibberellins during fruit and seed development: studies on gibberellin-deficient genotypes of *Arabidopsis thaliana*. Physiol Plant **67:** 315–319

Basu D, Liang Y, Liu X, Himmeldirk K, Faik A, Kieliszewski M, Held M, Showalter AM (2013) Functional identification of a hydroxyproline-o-galactosyltransferase specific for arabinogalactan protein biosynthesis in *Arabidopsis*. J Biol Chem **288:** 10132–10143

Basu D, Wang W, Ma S, DeBrosse T, Poirier E, Emch K, Soukup E, Tian L, Showalter AM (2015) Two hydroxyproline galactosyltransferases, GALT5 and GALT2, function in arabinogalactan-protein glycosylation, growth and development in Arabidopsis. PLoS One **10:** e0125624

Bradley DJ, Wood EA, Larkins AP, Galfre G, Butcher GW, Brewin NJ (1988) Isolation of monoclonal antibodies reacting with peribacteriod membranes and other components of pea root nodules containing *Rhizobium leguminosarum*. Planta **173:** 149–160

Caffall KH, Mohnen D (2009) The structure, function, and biosynthesis of plant cell wall pectic polysaccharides. Carbohydr Res **344:** 1879–1900

Chang HS, Zhang C, Chang YH, Zhu J, Xu XF, Shi ZH, Zhang XL, Xu L, Huang H, Zhang S, Yang ZN (2012) *No primexine and plasma membrane undulation* is essential for primexine deposition and plasma membrane undulation during microsporogenesis in Arabidopsis. Plant Physiol **158:** 264–272

Choi H, Jin JY, Choi S, Hwang JU, Kim YY, Suh MC, Lee Y (2011) An ABCG/WBC-type ABC transporter is essential for transport of sporopollenin precursors for exine formation in developing pollen. Plant J **65:** 181–193

Coimbra S, Almeida J, Junqueira V, Costa ML, Pereira LG (2007) Arabinogalactan proteins as molecular markers in *Arabidopsis thaliana* sexual reproduction. J Exp Bot **58:** 4027–4035

Coimbra S, Costa M, Jones B, Mendes MA, Pereira LG (2009) Pollen grain development is compromised in *Arabidopsis agp6 agp11* null mutants. J Exp Bot **60:** 3133–3142

Coimbra S, Costa M, Mendes MA, Pereira AM, Pinto J, Pereira LG (2010) Early germination of *Arabidopsis* pollen in a double null mutant for the arabinogalactan protein genes *AGP6* and *AGP11*. Sex Plant Reprod **23:** 199–205

de Azevedo Souza C, Kim SS, Koch S, Kienow L, Schneider K, McKim SM, Haughn GW, Kombrink E, Douglas CJ (2009) A novel fatty Acyl-CoA Synthetase is required for pollen development and sporopollenin biosynthesis in *Arabidopsis*. Plant Cell **21:** 507–525

Dobritsa AA, Geanconteri A, Shrestha J, Carlson A, Kooyers N, Coerper D, Urbanczyk-Wochniak E, Bench BJ, Sumner LW, Swanson R, Preuss D (2011) A large-scale genetic screen in Arabidopsis to identify genes involved in pollen exine production. Plant Physiol **157:** 947–970

Dobritsa AA, Lei Z, Nishikawa S, Urbanczyk-Wochniak E, Huhman DV, Preuss D, Sumner LW (2010) *LAP5* and *LAP6* encode anther-specific proteins with similarity to chalcone synthase essential for pollen exine development in Arabidopsis. Plant Physiol **153:** 937–955

Dobritsa AA, Nishikawa S, Preuss D, Urbanczyk-Wochniak E, Sumner LW, Hammond A, Carlson AL, Swanson RJ (2009a) *LAP3*, a novel plant protein required for pollen development, is essential for proper exine formation. Sex Plant Reprod **22:** 167–177

Dobritsa AA, Shrestha J, Morant M, Pinot F, Matsuno M, Swanson R, Møller BL, Preuss D (2009b) CYP704B1 is a long-chain fatty acid ω-hydroxylase essential for sporopollenin synthesis in pollen of Arabidopsis. Plant Physiol **151:** 574–589

Dong X, Hong Z, Sivaramakrishnan M, Mahfouz M, Verma DP (2005) Callose synthase (CalS5) is required for exine formation during microgametogenesis and for pollen viability in Arabidopsis. Plant J **42:** 315–328

Dou XY, Yang KZ, Zhang Y, Wang W, Liu XL, Chen LQ, Zhang XQ, Ye D (2011) WBC27, an adenosine tri-phosphate-binding cassette protein, controls pollen wall formation and patterning in Arabidopsis. J Integr Plant Biol **53:** 74–88

Egelund J, Ellis M, Doblin M, Qu Y, Bacic A (2011) Genes and enzymes of the GT31 family: towards unravelling the function(s) of the plant glycosyl transferase family members. Ann Plant Res **41:** 213–234

Ellis M, Egelund J, Schultz CJ, Bacic A (2010) Arabinogalactan-proteins: key regulators at the cell surface? Plant Physiol **153:** 403–419

Fincher GB, Stone BA, Clarke AE (1983) Arabinogalactan-proteins: structure, biosynthesis, and function. Annu Rev Plant Physiol **34:** 47–70

Geshi N, Johansen JN, Dilokpimol A, Rolland A, Belcram K, Verger S, Kotake T, Tsumuraya Y, Kaneko S, Tryfona T, Dupree P, Scheller HV, et al (2013) A galactosyltransferase acting on arabinogalactan protein glycans is essential for embryo development in Arabidopsis. Plant J **76:** 128–137

Grienenberger E, Kim SS, Lallemand B, Geoffroy P, Heintz D, Souza CdeA, Heitz T, Douglas CJ, Legrand M (2010) Analysis of *TETRAKETIDE α-PYRONE REDUCTASE* function in *Arabidopsis thaliana* reveals a previously unknown, but conserved, biochemical pathway in sporopollenin monomer biosynthesis. Plant Cell **22:** 4067–4083

Griffiths JS, Tsai AY, Xue H, Voiniciuc C, Šola K, Seifert GJ, Mansfield SD, Haughn GW (2014) SALT-OVERLY SENSITIVE5 mediates Arabidopsis seed coat mucilage adherence and organization through pectins. Plant Physiol **165:** 991–1004

Guan YF, Huang XY, Zhu J, Gao JF, Zhang HX, Yang ZN (2008) *RUPTURED POLLEN GRAIN1*, a member of the MtN3/saliva gene family, is crucial for exine pattern formation and cell integrity of microspores in Arabidopsis. Plant Physiol **147:** 852–863

Heslop-Harrison J (1968) Pollen wall development. The succession of events in the growth of intricately patterned pollen walls is described and discussed. Science **161:** 230–237

Hoedemaekers K, Derksen J, Hoogstrate SW, Wolters-Arts M, Oh SA, Twell D, Mariani C, Rieu I (2015) BURSTING POLLEN is required to organize the pollen germination plaque and pollen tube tip in *Arabidopsis thaliana*. New Phytol **206:** 255–267

Hu J, Wang Z, Zhang L, Sun MX (2014) The Arabidopsis *Exine Formation Defect* (*EFD*) gene is required for primexine patterning and is critical for pollen fertility. New Phytol **203:** 140–154

Immerzeel P, Eppink MM, de Vries SC, Schols HA, Voragen AGJ (2006) Carrot arabinogalactan proteins are interlinked with pectins. Physiol Plant **128:** 18–28

Ishiguro S, Nishimori Y, Yamada M, Saito H, Suzuki T, Nakagawa T, Miyake H, Okada K, Nakamura K (2010) The Arabidopsis *FLAKY POLLEN1* gene encodes a 3-hydroxy-3-methylglutaryl-coenzyme A synthase required for development of tapetum-specific organelles and fertility of pollen grains. Plant Cell Physiol **51:** 896–911

Jauh YG, Lord EM (1996) Localization of pectins and arabinogalactan-proteins in lily (*Lilium longiflorum* L.) pollen tube and style, and their possible roles in pollination. Planta **199:** 251–261

Jia QS, Zhu J, Xu XF, Lou Y, Zhang ZL, Zhang ZP, Yang ZN (2015) *Arabidopsis* AT-hook protein TEK positively regulates the expression of arabinogalactan proteins for Nexine formation. Mol Plant **8:** 251–260

Jiang J, Zhang Z, Cao J (2013) Pollen wall development: the associated enzymes and metabolic pathways. Plant Biol (Stuttg) **15:** 249–263

Kim SS, Grienenberger E, Lallemand B, Colpitts CC, Kim SY, Souza CdeA, Geoffroy P, Heintz D, Krahn D, Kaiser M, Kombrink E, Heitz T, et al (2010) *LAP6/POLYKETIDE SYNTHASE A* and *LAP5/POLYKETIDE SYNTHASE B* encode hydroxyalkyl α-pyrone synthases required for pollen development and sporopollenin biosynthesis in *Arabidopsis thaliana*. Plant Cell **22:** 4045–4066

Knox JP, Linstead PJ, King J, Cooper C, Roberts K (1990) Pectin esterification is spatially regulated both within cell walls and between developing tissues of root apices. Planta **181:** 512–521

Kuromori T, Ito T, Sugimoto E, Shinozaki K (2011) *Arabidopsis* mutant of AtABCG26, an ABC transporter gene, is defective in pollen maturation. J Plant Physiol **168:** 2001–2005

Lampugnani ER, Ho YY, Moller IE, Koh PL, Golz JF, Bacic A, Newbigin E (2016) A glycosyltransferase from *Nicotiana alata* pollen mediates synthesis of a linear (1,5)-α-L-arabinan when expressed in Arabidopsis. Plant Physiol **170:** 1962–1974

Lampugnani ER, Kilinc A, Smyth DR (2012) *PETAL LOSS* is a boundary gene that inhibits growth between developing sepals in *Arabidopsis thaliana*. Plant J **71:** 724–735

Li WL, Liu Y, Douglas CJ (2017) Role of glycosyl transferases in pollen wall primexine formation and exine patterning. Plant Physiol **173:** 167–182

Li Y-Q, Faleri C, Geitmann A, Zhang H-Q, Cresti M (1995) Immunogold localization of arabinogalactan proteins, unesterified and esterified pectins in pollen grains and pollen tubes of *Nicotiana tabacum* L. Protoplasma **189:** 26–36

Ling NXY, Lee J, Ellis M, Liao M-L, Mau S-L, Guest D, Janssen PH, Kováč P, Bacic A, Pettolino FA (2012) An *exo*-β-(1→3)-D-galactanase from *Streptomyces* sp. provides insights into type II arabinogalactan structure. Carbohydr Res **352:** 70–81

Majewska-Sawka A, Münster A, Wisniewska E (2004) Temporal and spatial distribution of pectin epitopes in differentiating anthers and microspores of fertile and sterile sugar beet. Plant Cell Physiol **45:** 560–572

Majewska-Sawka A, Rodriguez-Garcia MI (2006) Immunodetection of pectin and arabinogalactan protein epitopes during pollen exine formation of *Beta vulgaris* L. Protoplasma **228:** 41–47

McGill NW, Williams SJ (2009) 2,6-Disubstituted benzoates as neighboring groups for enhanced diastereoselectivity in β-galactosylation reactions: synthesis of β-1,3-linked oligogalactosides related to arabinogalactan proteins. J Org Chem **74:** 9388–9398

Micheli F (2001) Pectin methylesterases: cell wall enzymes with important roles in plant physiology. Trends Plant Sci **6:** 414–419

Mohnen D (2008) Pectin structure and biosynthesis. Curr Opin Plant Biol **11:** 266–277

Mollet JC, Kim S, Jauh GY, Lord EM (2002) Arabinogalactan proteins, pollen tube growth, and the reversible effects of Yariv phenylglycoside. Protoplasma **219:** 89–98

Morant M, Jørgensen K, Schaller H, Pinot F, Møller BL, Werck-Reichhart D, Bak S (2007) CYP703 is an ancient cytochrome P450 in land plants catalyzing in-chain hydroxylation of lauric acid to provide building blocks for sporopollenin synthesis in pollen. Plant Cell **19:** 1473–1487

Nakagawa T, Nakamura S, Tanaka K, Kawamukai M, Suzuki T, Nakamura K, Kimura T, Ishiguro S (2008) Development of R4 gateway binary vectors (R4pGWB) enabling high-throughput promoter swapping for plant research. Biosci Biotechnol Biochem **72:** 624–629

Nakagawa T, Suzuki T, Murata S, Nakamura S, Hino T, Maeo K, Tabata R, Kawai T, Tanaka K, Niwa Y, Watanabe Y, Nakamura K, et al (2007) Improved Gateway binary vectors: high-performance vectors for creation of fusion constructs in transgenic analysis of plants. Biosci Biotechnol Biochem **71:** 2095–2100

Newbigin E, Bacic A, Read S (2009) Callose and its role in pollen and embryosac development in flowering plants. *In* Bacic A, Fincher G B, Stone B A, eds, Chemistry, Biochemistry and Biology of (1,3)-β-Glucans and Related Polysaccharides. Academic Press, Elsevier, New York, pp 465–498

Nguema-Ona E, Coimbra S, Vicré-Gibouin M, Mollet J-C, Driouich A (2012) Arabinogalactan proteins in root and pollen-tube cells: distribution and functional aspects. Ann Bot (Lond) **110:** 383–404

Nishikawa S, Zinkl GM, Swanson RJ, Maruyama D, Preuss D (2005) Callose (β-1,3 glucan) is essential for *Arabidopsis* pollen wall patterning, but not tube growth. BMC Plant Biol **5:** 22

Ogawa-Ohnishi M, Matsubayashi Y (2015) Identification of three potent hydroxyproline *O*-galactosyltransferases in Arabidopsis. Plant J **81:** 736–746

Owen HA, Makaroff CA (1995) Ultrastructure of microsporogenesis and microgametogenesis in *Arabidopsis thaliana* (L.) Heynh. ecotype Wassilewskija (Brassicaceae). Protoplasma **185:** 7–21

Paxson-Sowders DM, Dodrill CH, Owen HA, Makaroff CA (2001) DEX1, a novel plant protein, is required for exine pattern formation during pollen development in Arabidopsis. Plant Physiol **127:** 1739–1749

Paxson-Sowders DM, Owen HA, Makaroff CA (1997) A comparative ultrastructural analysis of exine pattern development in wild-type *Arabidopsis* and a mutant defective in pattern formation. Protoplasma **198:** 53–65

Peiffer JA, Kaushik S, Sakai H, Arteaga-Vazquez M, Sanchez-Leon N, Ghazal H, Vielle-Calzada J-P, Meyers BC (2008) A spatial dissection of the Arabidopsis floral transcriptome by MPSS. BMC Plant Biol **8:** 43

Pelloux J, Rustérucci C, Mellerowicz EJ (2007) New insights into pectin methylesterase structure and function. Trends Plant Sci **12:** 267–277

Pennell RI, Janniche L, Kjellbom P, Scofield GN, Peart JM, Roberts K (1991) Developmental regulation of a plasma membrane arabinogalactan protein epitope in oilseed rape flowers. Plant Cell **3:** 1317–1326

Pereira AM, Pereira LG, Coimbra S (2015) Arabinogalactan proteins: rising attention from plant biologists. Plant Reprod **28:** 1–15

Qu Y, Egelund J, Gilson PR, Houghton F, Gleeson PA, Schultz CJ, Bacic A (2008) Identification of a novel group of putative *Arabidopsis thaliana* β-(1,3)-galactosyltransferases. Plant Mol Biol **68:** 43–59

Quilichini TD, Douglas CJ, Samuels AL (2014) New views of tapetum ultrastructure and pollen exine development in *Arabidopsis thaliana*. Ann Bot (Lond) **114:** 1189–1201

Quilichini TD, Friedmann MC, Samuels AL, Douglas CJ (2010) ATP-binding cassette transporter G26 is required for male fertility and pollen exine formation in Arabidopsis. Plant Physiol **154:** 678–690

Quilichini TD, Grienenberger E, Douglas CJ (2015) The biosynthesis, composition and assembly of the outer pollen wall: a tough case to crack. Phytochemistry **113:** 170–182

Rhee SY, Somerville CR (1998) Tetrad pollen formation in *quartet* mutants of *Arabidopsis thaliana* is associated with persistence of pectic polysaccharides of the pollen mother cell wall. Plant J **15:** 79–88

Shi J, Cui M, Yang L, Kim YJ, Zhang D (2015) Genetic and biochemical mechanisms of pollen wall development. Trends Plant Sci **20:** 741–753

Showalter AM, Basu D (2016) Extensin and arabinogalactan-protein biosynthesis: glycosyltransferases, research challenges, and biosensors. Front Plant Sci **7:** 814

Smyth DR, Bowman JL, Meyerowitz EM (1990) Early flower development in *Arabidopsis*. Plant Cell **2:** 755–767

Song L, Zeng W, Wu A, Picard K, Lampugnani ER, Cheetamun R, Beahan C, Cassin A, Lonsdale A, Doblin MS, Bacic A (2015) *Asparagus* spears as a model to study heteroxylan biosynthesis during secondary wall development. PLoS One **10:** e0123878

Strasser R, Bondili JS, Vavra U, Schoberer J, Svoboda B, Glössl J, Léonard R, Stadlmann J, Altmann F, Steinkellner H, Mach L (2007) A unique β1,3-galactosyltransferase is indispensable for the biosynthesis of *N*-glycans containing Lewis a structures in *Arabidopsis thaliana*. Plant Cell **19:** 2278–2292

Sun MX, Huang XY, Yang J, Guan YF, Yang ZN (2013) Arabidopsis RPG1 is important for primexine deposition and functions redundantly with RPG2 for plant fertility at the late reproductive stage. Plant Reprod **26:** 83–91

Suzuki T, Masaoka K, Nishi M, Nakamura K, Ishiguro S (2008) Identification of *kaonashi* mutants showing abnormal pollen exine structure in *Arabidopsis thaliana*. Plant Cell Physiol **49:** 1465–1477

Tan L, Eberhard S, Pattathil S, Warder C, Glushka J, Yuan C, Hao Z, Zhu X, Avci U, Miller JS, Baldwin D, Pham C, et al (2013) An *Arabidopsis* cell wall proteoglycan consists of pectin and arabinoxylan covalently linked to an arabinogalactan protein. Plant Cell **25:** 270–287

Tan L, Showalter AM, Egelund J, Hernandez-Sanchez A, Doblin MS, Bacic A (2012) Arabinogalactan-proteins and the research challenges for these enigmatic plant cell surface proteoglycans. Front Plant Sci **3:** 140

Tang LK, Chu H, Yip WK, Yeung EC, Lo C (2009) An anther-specific dihydroflavonol 4-reductase-like gene (*DRL1*) is essential for male fertility in Arabidopsis. New Phytol **181:** 576–587

van Aelst AC, van Went JL (1992) Ultrastructural immuno-localization of pectins and glycoproteins in *Arabidopsis thaliana* pollen grains. Protoplasma **168:** 14–19

Voiniciuc C, Günl M, Schmidt MH, Usadel B (2015) Highly branched xylan made by IRREGULAR XYLEM14 and MUCILAGE-RELATED21 links mucilage to Arabidopsis seeds. Plant Physiol **169:** 2481–2495

Wallace S, Fleming A, Wellman CH, Beerling DJ (2011) Evolutionary development of the plant and spore wall. AoB Plants **2011:** plr027

Weigel D, Glazebrook J (2002) Arabidopsis: A Laboratory Manual. Cold Spring Harbor Laboratory Press, Cold Spring Harbor, NY.

Wilson SM, Bacic A (2012) Preparation of plant cells for transmission electron microscopy to optimize immunogold labeling of carbohydrate and protein epitopes. Nat Protoc **7:** 1716–1727

Wilson SM, Ho YY, Lampugnani ER, van de Meene AML, Bain MP, Bacic A, Doblin MS (2015) Determining the subcellular location of synthesis and assembly of the cell wall polysaccharide (1,3; 1,4)-β-D-glucan in grasses. Plant Cell **27:** 754–771

Wolf S, Greiner S (2012) Growth control by cell wall pectins. Protoplasma **249**(Suppl 2): S169–S175

Wu Y, Yan J, Zhang R, Qu X, Ren S, Chen N, Huang S (2010) *Arabidopsis* FIMBRIN5, an actin bundling factor, is required for pollen germination and pollen tube growth. Plant Cell **22:** 3745–3763

Zhou Q, Zhu J, Cui Y-L, Yang Z-N (2015) Ultrastructure analysis reveals sporopollenin deposition and nexine formation at early stage of pollen wall development in *Arabidopsis*. Science Bulletin **62:** 273–276